Replies to both referee comments are contained in this document. Referee comments are in black, and our responses in blue. Modifications to the manuscript are in italics, with the line number (for the revised manscript) in bold.

Reply to RC1

Global comments :
The authors present results of the IAOOS field experiment which took place from 2014and 2019 in the central Arctic. They focus on lidar measurements which were performed on drifting buoys and analyse cloud occurrence and further cloud propertiesbased on this data set. They also look into the radiative fluxes measured during theN-ICE campaign, where collocated buoy observations were made as well, and analyse the different radiative modes observed in this time period. Here, they compare the observations to ERA5 reanalysis data.

Enhancing cloud observations in the Arctic is crucial to better understand Arctic clouds,they radiative impact and their impact on the Arctic climate system. Especially in the harsh Arctic environment and especially in the Central Arctic, it is quite challengingto acquire such data. Using drifting buoys with such instrumentation is quite impressive. The authors discuss the challenges of such observations and also the limitations.
However, also the retrieved data is limited and lacks spatial (as the authors mention) and temporal coverage. This needs to be kept in mind when analysing and discussing the data. A maximum of 4 lidar profiles per day cannot provide robust cloud statistics. However, this is how the authors sell the results. In particular, monthly statistics based on this data, in particular for those months where the number of profiles is even less than 100, don't seem to be reliable. At ground-based surface observatories, continuous observations can be performed. Assuming a typical 1-min resolution of lidar measurement, this would result in at least 1440 profiles per day. What if only 4 measurements, i.e. 4 random snapshots of clouds at one day, were available instead? Would they capture the cloud statistics based on the high-resolution data? Don't get me wrong: I think that this data set is of high value but the representativity needs to be critically discussed. This is partly done in the manuscript but needs to be enhanced.

During the N-ICE campaign, a micropulse lidar (MPL) is available. I strongly suggest to also include a section showing the comparison between the results of the buoy lidar and the MPL. This would provide more insight in the representativeness of the buoy lidar cloud observations. Please find in addition my specific comments below.

First of all, we would like to thank the reviewer for his comments, which are both detailed and pertinent, as well as for the suggested references. We are sensible of the time and effort which must have been spent in reviewing the manuscript in this way.

Firstly, we will address the reviewer's main points, which we understand to be :
- that the statistics lack robustness due to the low number of points, especially in the months of October, November, December, March and April ;
- that a maximum of 4 profiles/day may not be representative of the higher-resolution cloud statistics ;
- and that therefore the robustness and representativity of the IAOOS lidar profiles must be critically discussed, in order to avoid overstating the results. The reviewer suggests that we compare our data with that of the MPL available during the N-ICE campaign.

We fully agree that a critical discussion of these points is necessary.

Robustness

The number of lidar profiles yielded by the IAOOS buoys is naturally lower than that at a ground based station, because the buoys are autonomous and therefore have a limited power supply and no supervision by an operator. In particular, as noted by the reviewer, there were less than 100 profiles/month for the October – April period. This is due to the especially harsh winter conditions. It naturally creates uncertainty on the calculated monthly cloud statistics. However, the seasonal variability appears robust, i.e. distributions of cloud properties do in general differ at a stastically significant level between summer and April, November, and December.

Here, we will discuss the cloud occurrence frequency in particular, as the reviewer notes in his specific comments that the low cloud frequencies in the months of November/December and March/April are suspicious, and we believe this to be an important result of the paper.

Putting aside the number of profiles for the moment, the reviewer's comments indicate that the obtained cloud frequencies (56 % in November, 32 % in December, 46 % in May and 59 % in April) are inherently suspicious because they are too low. We are surprised by this assessment. With the exception of December, the obtained values are within the envelope of previous studies, even from ground-based observations (Shupe et al, 2011 ; Wang and Key, 2004 ; Zygmuntowska, 2012).

In order to make our case more rigorously, we have calculated 90 % confidence intervals on the obtained monthly cloud occurrence frequencies. This is done in the following way, for each month :

- We suppose that the event "presence of a cloud with base<2 km in a given IAOOS lidar profile" has a probability p, with p the cloud frequency. Since the profiles are at least 6h apart, the events can be considered to be independent. Then, the number of profiles in each month which contain at least one cloud follows a binomial distribution with parameters p and n (n is the total number of profiles in a month).

- The probability distribution of p, taking into account our monthly measurements, can then be calculated from an a priori distribution using the Bayes formula. In practice, the a priori distribution doesn't have a great impact ; based on values found in the literature, we have chosen a normal distribution centered on 0.7.

- The 5th and 95th percentiles of this probability distribution can be calculated to obtain a 90 % confidence interval for p (e.g., 29 % - 51 % for December).

This method is further explained in Appendix A to the revised manuscript.

The probability distributions for the months of May to October show significant overlap (Fig. 1). However, they do not overlap at all with the November, December, March and April distributions, although these are much wider because of the lower number of measurements. We contend that the IAOOS measurements do therefore show significant seasonal variability in cloud frequency between winter and summer, with a transition between October and November and April and May.

For other cloud quantities we have applied the Mann-Whitney U test to show that there are statistically significant differences between months (see revised manuscript).

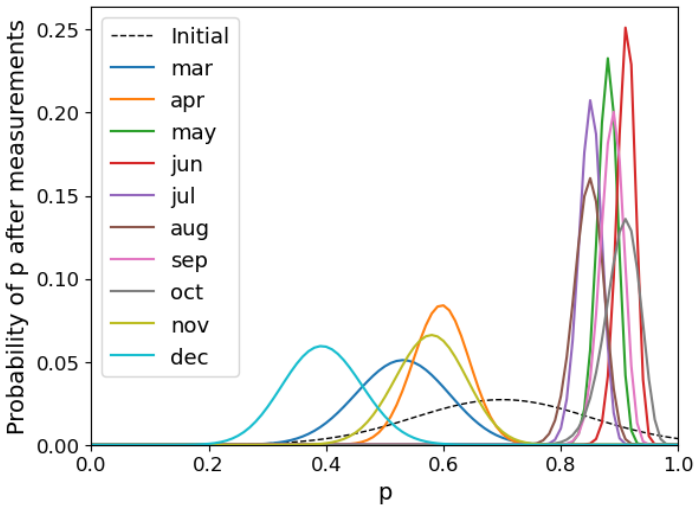

Fig. 1 : Monthly probability distributions of p after the measurements are taken into account (the dashed line is the a priori distribution, which is the same for each month).

Representativity

The other main difficulty expressed by the reviewer pertained to the representativity of the IAOOS time sampling. The choice was made for the IAOOS campaign to have the lidar shoot only every six hours and sometimes less, depending on conditions and the need to preserve battery power. This was of course partly for practical reasons – it would have been impossible for the lidar to shoot every minute. But it is also part of the approach. Similar to worldwide radiosonde launches which occur every 12 hours, one lidar profile every six hours is assumed to represent a random sample of cloud conditions over the buoy operation period.

This approach can, and should, be discussed.
1) Shooting at a given time only four times/day may also induce a bias in the resulting statistics if there is a strong diurnal variability in cloud cover. To give an extreme example : a sample of profiles acquired at 3 UTC and 9 UTC would obviously not be representative if clouds only ever occurred between 3:30 UTC and 8:30 UTC.
2) Whether or not one profile every six hours is enough to represent cloud statistics naturally depends on the timescale of cloud variations. For another extreme example, there would be no point in sampling at a 1 minute resolution if clouds maintained themselves for months at a time.

To answer the first point : in general, there is little diurnal cycle at high latitudes, since the shortwave radiation varies more on a seasonal than on a daily scale. This is supported by the literature. Analysing data from six Arctic ground stations, Shupe et al. (2011) found that on average, the cloud occurrence anomaly from the daily mean was less than 5 percentage points. Our opinion is that the lidar sampling at constant times does not induce any strong bias in the statistics.

As to the second point, the 6-12h sampling timestep must be compared to the timescales of cloud variability in the Arctic. Shupe et al. (2011) analysed the temporal persistence of cloud layers in the Arctic from data at six Arctic ground stations. They found that median cloud persistence ranges between 3.1 to 4.5h among the studied sites, while the mean varies from 8 to 22h. These values are of the same order as the IAOOS time step, so we expect that the sampling should not produce large errors.

We generated random series of alternating cloudy/clear periods from lognormal distributions which respect the means and medians of Shupe et al. These series each had a total length of 744h, or 31 days. The mean cloud occurrence frequency (COF) over each random series was then calculated using different sampling timesteps, from

1 min to 48h. The results were compared to the COF calculated with a timestep of 1 min.

Over a total of 300 such random series, the highest absolute error (top 5th percentile) incurred on COF by a sampling timestep of 12h was around 8 %. For a timestep of 6h, this value was only 5 %. In fact, it appears that it is not necessary to sample at very high temporal resolution in order to get a good picture of the overall cloud occurrence frequency.

The reviewer suggested comparing the IAOOS lidar data with the N-ICE MPL, which had a 1-min timestep, to see if a 6h sampling timestep correctly reproduces the cloud statistics. This is an interesting idea, but nothing guarantees that such a case study would in turn be representative. We believe the above explanation is quantitatively more robust.

Specific comments:

l 5: “Cloud frequency is globally at 75%...”: unclear what globally means. please be more specific (which time period exactly, region).
« Globally » here means the April – December average over the whole campaign period. The text has been edited to make this clearer and now reads :

(l 5) *The average cloud frequency from April to December over the course of the campaign was 75%. Cloud occurrence frequencies were above 85% from May to October.*

l7: “On the whole, the cloud cover is very low...”. Misleading. Could be read as: Cloudcover (=cloud fraction) is low (=small). Rather use “Cloud base height is very low...”
This has been edited accordingly.

ll 26 ff: You could also mention the results of Mioche, G., Jourdan, O., Ceccaldi, M.,and Delanoë, J.: Variability of mixed-phase clouds in the Arctic with a focus on the Svalbard region: a study based on spaceborne active remote sensing, Atmos. Chem.Phys., 15, 2445–2461, https://doi.org/10.5194/acp-15-2445-2015, 2015

ll 41: Concerning ground-based cloud observations, you could mention the studies by

Shupe, M. D., V. P. Walden, E. Eloranta, T. Uttal, J. R. Campbell, S. M. Starkweather,and M. Shiobara, 2011: Clouds at Arctic Atmospheric Observatories. Part I: Oc-currence and Macrophysical Properties. J. Appl. Meteor. Climatol., 50, 626–644, https://doi.org/10.1175/2010JAMC2467.1.

and

Shupe, M. D., 2011: Clouds at Arctic Atmospheric Observatories. Part II: Ther-modynamic Phase Characteristics.J. Appl.Meteor.Climatol., 50, 645–661,https://doi.org/10.1175/2010JAMC2468.1.

Also, be aware of the enhanced cloud observations at Ny-Ålesund:

Nomokonova, T., Ebell, K., Löhnert, U., Maturilli, M., Ritter, C., and O’Connor,E.: Statistics on clouds and their relation to thermodynamic conditions at Ny-Ålesund using ground-based sensor synergy, Atmos. Chem. Phys., 19, 4105–4126, https://doi.org/10.5194/acp-19-4105-2019, 2019.

Ebell, K., T. Nomokonova, M. Maturilli, and C. Ritter, 2020: Radiative Effect of Clouds at Ny-Ålesund, Svalbard, as Inferred from Ground-Based Remote Sensing Observations.J. Appl. Meteor. Climatol., 59, 3–22, https://doi.org/10.1175/JAMC-D-19-0080.1.

ll 45 ff: concerning shipborne and airborne observations it is also worth mentioning the ACLOUD and PASCAL campaigns:

Wendisch, M., and Coauthors, 2019: The Arctic Cloud Puzzle: Using ACLOUD/PASCAL Multiplatform Observations to Unravel the Role of Clouds and Aerosol Particles in Arctic Amplification. Bull. Amer. Meteor. Soc., 100, 841–871, https://doi.org/10.1175/BAMS-D-18-0072.1.

Thank you for the references. They have been cited in the revised manuscript.

l 64: ”extract a 5-year statistics of the Arctic cloud cover”: This is overstated. It hast o be made clear that this is not a robust statistic with respect to spatial and temporal coverage. Be more precise here: e.g. “cloud cover along the track of the drifting buoys in the central Arctic for the months of . . .”
We agree that the shortcut used led to an overstatement of the scope of the dataset. We have amended this sentence to:

(l 66) *...to extract a multi year statistic of the April to December cloud cover along the track of the drifting buoys.*

l 89: As mentioned before, having only a maximum of four lidar measurements per day is a very, very low number. The representativity needs to be critically discussed. Not only once, but also when presenting the results.
This point has been discussed in the general answer above. Having only four profiles a day was partly due to measurement constraints, but it was also a methodological choise as one lidar profile every six hours is assumed to represent a random sample of cloud conditions. Indeed, because clouds persist on average from 8h to 22h, it is not necessary to have one profile per minute in order to measure monthly values of cloud occurrence frequency.

l 101: “red line”: ambiguous, better “red circle”
This has been edited accordingly.

ll 106: information on N-ICE campaign: Please include more information about the campaign data set and the auxiliary instrum entation, e.g. detailed information about the radiation sensors (“four component radiometer”). What kind of instruments exactly? What are the instrument specifications ? I assume they both down- and upward radiative fluxes are provided, right? Where is the instrumentation exactly installed? Distance of the instruments to each other? Why is the information of the MPL not used in addition? The measurements of the MPL should be set in to context to the buoy lidar observations.
We have added more information about the campaign dataset and the instruments. This paragraph now reads :

(l 109) *The Norwegian Young Sea Ice Experiment (N-ICE) campaign took place from January to June 2015. During that time, theresearch vessel Lance drifted with four different ice floes (Walden et al.; Cohen et al., 2017; Walden et al., 2017). The first two drifts took place during the winter (January - March 2015) while the last two drifts occurred in the late spring to early summer period (April to June 2015). On each floe, a "Supersite" ice camp was installed about 300m away from the research vessel. Atmospheric measurements were mostly performed at this Supersite. Surface*

longwave fluxes (up and down) were measured with a Kipp & Zonen CGR4 pyrgeometer, which has a 4.5 to 42 µm bandwith. The shortwave fluxes (up and down) were measured with a Kipp & Zonen CMP22 pyranometer (200 to 3600 nm bandwidth). Both these instruments were heated and ventilated using a Kipp & Zonen CVF4 unit. Their accuracy is 3% (or 5 W m^{-2}) for the shortwave, and 2% (or 3 W m^{-2}) for the longwave (Walden et al., 2017; Hudson et al., 2016). The temperature at two meters was measured with a ventilated and shielded Vaisala HMP-155A sensor which has an accuracy of 2.4% (or 0.3°C) (Graham et al., 2017; Cohen et al., 2017). In addition, radiosondes were launched twice-daily from the research vessel, yielding profiles of relative humidity, temperature and wind speed (Walden et al., 2017).
Four IAOOS buoys were deployed during this campaign and drifted in the ice floe close to the research vessel. In particular, the B12 buoy was locked into the third ice floe 200m away from the Supersite from end of April to the beginning of June 2015 (Fig. 1). Because of the proximity of the buoy to the Supersite over this period, the N-ICE surface radiative flux and temperature measurements can be used as a complement to the IAOOS data. This allowed us to evaluate the radiative impact of clouds on the surface in late spring to early summer (Sect. 5.2.1 and 5.3).

Our reasons for not using the MPL as a comparison to the lidar buoy has been discussed above.

l 111: “April to June”, please add 2015
This section has been modified as shown in the above paragraph.

l 114: please provide a reference for ERA-5
The following reference has been added :

Hersbach, H., Bell, B., Berrisford, P., Hirahara, S., Horányi, A., Muñoz-Sabater, J., Nicolas, J., Peubey, C., Radu, R., Schepers, D., Simmons,A., Soci, C., Abdalla, S., Abellan, X., Balsamo, G., Bechtold, P., Biavati, G., Bidlot, J., Bonavita, M., Chiara, G., Dahlgren, P., Dee,D., Diamantakis, M., Dragani, R., Flemming, J., Forbes, R., Fuentes, M., Geer, A., Haimberger, L., Healy, S., Hogan, R. J., Hólm, E.,620Janisková, M., Keeley, S., Laloyaux, P., Lopez, P., Lupu, C., Radnoti, G., Rosnay, P., Rozum, I., Vamborg, F., Villaume, S., and Thépaut, J.-N.: The ERA5 global reanalysis, Quarterly Journal of the Royal Meteorological Society, 146, 1999–2049, https://doi.org/10.1002/qj.3803,2020.

l 116: “L1”? Please be more specific
The L1 marked a bibliography reference to the link for acquiring ERA5 data on the ECMWF website. This was indeed quite unclear, and it has been updated to the following :
(l 129) *(Copernicus Climate Change Service (C3S), 2017)*

ll 122 ff: How does the lidar window frost impact cloud detection? You could state at the end of section 3.1.1 what this means for the accuracy of the cloud observations?
As noted in this section, the frost modifies the system constant C (by lowering the window transmission). Once the modified C is determined using the method outlined in this section, it is plugged in to the attenuated scattering ratio (SRatt) calculation. The obtained SRatt should therefore be independent of window frost and there should be no further impact on cloud detection.

Of course, the modified C determined through this method may be slightly off. Mariage (2015) estimates that the error on C is around 30 % for a frost index between 0,1 and 0,3. The impact of cloud detection then depends on the sign of the error. If C is erroneously high, for example, SRatt will be erroneously low. This would lead to features being harder to detect (and therefore, feature bases being too high). On the

other hand, if C is erroneously low, SRatt will be erroneously high and spurious features may be detected.

In practice, visual inspection of the profiles indicates that the cloud detection algorithm is robust to the errors caused by the window frost correction. However, it is difficult to quantify the impact on the cloud observations.

We have added the following comments at the end of section 3.1.1 :
(l 151) *[…] this frost correction method naturally causes uncertainty on the obtained value of C. Around 11% of profiles have values of γ between 0.1 and 0.3. In this case, Mariage (2015) estimates that the window frost correction leads to a 30% error onC. A further 3%of profiles have 0.05≤γ <0.1, in which case the error on C can be up to 60%. For γ≥0.3, the C error tends towards the frost-free system constant determination error, which is around 10% (Mariage, 2015). The system constant is used in the calculation of the attenuated scattering ratio,from which all cloud quantities are derived (Sect. 3.2). However, it is difficult to quantify the impact of its error on cloud detection, in part because it depends on the sign of the error. An overestimated C would lead to under-detection of cloud layers, and vice versa. In practice, visual inspection of the profiles indicates that the cloud detection algorithm outlined below is robust to the errors that may be incurred during the window frost correction.*

l 160: Equation 1: please introduce all variables!
This has been corrected.

l 174: How is the threshold of 1.1 chosen? What is the impact on cloud detection?
In the absence of clouds (or aerosols) the attenuated scattering ratio (SRatt) should be 1 near the ground. Setting the threshold at 1.1 allows for a 10 % margin to avoid small fluctuations of the system constant C from « triggering » the algorithm into detecting a feature where there is none.

Setting the threshold lower therefore risks detecting spurious features. Setting the threshold higher would make it harder to detect a feature base. The algorithm would then risk either overestimating the altitude of the feature base, or missing the feature altogether (if it is thin). From visual inspection of the profiles, 1.1 appeared to be a good compromise.

Note that cloud layers, as opposed to aerosols, have large SRatt values. At the cloud base, SRatt increases very rapidly to values often >100. In practice, therefore, the specific value of the threshold (from 1.1 to 1.5, for example) has little impact on detection of cloud layers or on the determination of their base.

l 190 Tc has not been introduced
The text has been amended to introduce Tc (which is the cloud transmission).

l 192: Equation 2: make sure that all variables are introduced, e.g. alpha_p
Thank you for catching this. alpha_p was introduced right after Equation 2.

l 224: “Global” is misleading: Why not simply name it as it is: “average monthly cloud cover from March to December”
The suggested change was made.

ll 228 ff: just a comment here: low clouds frequently occur in the Arctic and it is especially difficult for satellites to capture these clouds also from active instrumentation,e.g. due to blind zone, ground clutter. Ground-based observations are thus crucial to capture these low clouds. It is true that for ground-based observations

the sensitivity is highest in the lower atmosphere but the combination of cloud radar and lidar can very well capture the whole atmospheric column! →(ll 235-236).
We thank the reviewer for this comment.

ll 236: which instruments were used in the Hahn et al study?
The Hahn et al study relies on surface weather reports from ships and ice camps, i.e. visual inspection of the sky. Naturally, these are quite uncertain in the dark, and the object of the study is to account for this issue by introducing a nighttime correction factor.

The text has been updated to note this point:
(l 261) *Averaging visual observations from ships and ice-camps, Hahn et al [...]*

ll 240-251 and Fig.2: You really need to discuss your results in conjunction with the number of measurements (as seen also in Table 2). The very low cloud occurrence in March, April, November and December is very suspicious. I would not overinterpret the results here. Please consider the representativity of the data. Discussion of "Inter-annual variability": I would also be careful here. I am not convinced that based on the number of data, any conclusions can be drawn here.
This point has been discussed in the general answer. We agree with the reviewer, however, that these paragraphs required further justification and that some conclusions should have been more careful.
We decided to eliminate references to March data throughout the manuscript, since this month had less than 30 profiles. We have changed ll 240-255 to the following paragraphs to clarify our reasoning and modulate our conclusions :

(l 266) *The results of IAOOS dataset are shown in Table 3 and Fig. 2. Note here that the number of profiles available for each month is variable, both because of the more favorable operation conditions in the summer and the timing of the buoy deployment (usually in May). As such, there are more than 200 profiles from May to September, around 100 in April and October, and less than 54 in November and December. Months with less than 30 profiles, i.e. January, February, and March, are not treated in this article. Care must therefore be taken in analysing the results of late autumn and winter. A 90% confidence interval for the cloud occurrence frequency can be estimated from a Bayesian calculation, assuming that the number of cloudy profiles followsa binomial distribution and supposing an appropriate a priori distribution for the cloud frequency from the literature (Appendix A).*

The IAOOS data shows a similar trend as the literature, with generally higher cloud cover values. From May to October, clouds are present over 85% of the time (Fig. 2). In contrast to the previous ground-based climatologies outlined above, there are two peaks at more than 0.9 in the monthly cloud frequency, although they differ little from the summer baseline. The first is in June, which has a mean cloud frequency of 0.92 and a confidence interval of (0.88−0.94). The second peak is in October, also with a mean cloud frequency of 0.92 but with a slightly wider confidence interval (0.85−0.95) because of the lower number of profiles. This is reminiscent of the results of Zygmuntowska et al. (2012), from CALIPSO data, which show a peak in cloud occurrence above 0.9 in October. July and August have slightly lower cloud frequency values (0.85 (0.82−0.88) and 0.85 (0.8−0.89) respectively). However, since there is non negligible overlap between the confidence intervals of June/October and the other summer months, it is difficult to draw solid conclusions as to May - October variability.

In the IAOOS dataset, April and November appear to mark a sharp transition in cloud occurrence frequency from the summer values. April has a cloud frequency of 0.59 (0.52−0.67) while the cloud frequency in November is 0.56 (0.48−0.68). While the confidence intervals are quite wide here due to the lower number of profiles, there is

no overlap with the summer confidence intervals. This suggests that the lower cloud frequencies observed during the months of April and November is meaningfully different from that of the months of May through October. December cloud frequency is lower still, at 0.32 (0.29−0.51). Note however the width of the confidence interval and the fact that the December data corresponds to a single year of measurement (2017).

It is not possible to robustly quantify interannual variability in Arctic cloud cover from the IAOOS dataset since there are at most four years of data for each month. Qualitatively, however, the April - May transition in cloud frequency observed by the buoys is quite variable. In 2014, the B02 buoy observed a very sharp spring transition in cloud frequency: from 40% (35%,60%) in April 2014 to more than 90% (89%,97%) in May and June 2014 (blue circles, Fig. 2). On the other hand, this transition was much more gradual in 2017 (buoy B24, orange diamonds). The June 2017 cloud frequency is less than 80% (69%,85%), overlapping significantly with the May 2017 cloud frequency confidence interval of (56%,78%). This is not an effect of spatial variability as both B02 and B24 were drifting in the Atlantic sector of the Arctic (Fig. 1).

l 256: “lacks spatial coverage”: but also temporal coverage! Again, a comparison between MPL data and the buoy lidar data are crucial to give more confidence in the temporal representativity of the results. You really need to draw your conclusions more carefully.
The part on spatial variability was simplified further and clarified. Our answer as to temporal representativity was given in the general comments.

(l 297) *It has been observed from satellite data that the Atlantic sector is the cloudiest part of the Arctic Ocean (Liu et al., 2012; Wang and Key, 2004). This is linked to the low pressure systems and the storm tracks arriving from the northern Atlantic Ocean. Since most of the IAOOS buoys drifted in this sector, the IAOOS dataset must be regarded as most representative of these specific conditions, and not of the ocean-wide cloud characteristics.*

Table 2: Are the numbers in each months are for all buoy drifts/years?
Yes. The caption has been edited to specify this :

[…] N_p is the total number of lidar profiles for each month ***(for all years and buoys)****.*

l 270: “non-significant”: did you perform a significance test?
No. We used « non-significant » here in its meaning of « insignificant », i.e. small. We acknowledge that this makes the statement confusing as « non-significant » in this context would most likely be interpreted in its statistical meaning.
However, the statistical significance question is interesting. Using Fisher’s exact test, the November multilayered cloud occurrence can be shown to be different from the July value at a statistically significant level (p-value = 0.007 for a two-sided alternative hypothesis) - despite the low number of profiles.

This has been reworded to :

(l 313) *Only one IAOOS profile contained multilayered clouds in November, and none in December. Despite the low number of total profiles in these months, these values are different from the July multilayered cloud frequency at a statistically significant level; for November, Fisher’s exact test yields a p-value of 0.007(Fisher, 1922).*

l 277: This is a too strong statement. Please rewrite.
This has been rewritten to :

(l 323) *Clouds in the IAOOS dataset are extremely low, with little seasonal variability [...]*

l 281: "(note however...)". Thank you that you mentioned that point here but not sufficiently discussed and highlighted.
The two sentences preceding l 281, i.e.

« [...] In March, only 57% of cloud bases are below 120 m. Another 29% of first layer cloud bases are between 120 and 500 m, which still corresponds to low level, likely boundary layer clouds (note however the low number of profiles in this month). »

have been removed, as we have decided not to treat the March data due to the low number of points.

l 286: "significant difference": tested?
Yes. The Mann-Whitney U test (for difference between the means of two independent samples) gives the following results :
- July (n1 = 355) and October (n2 = 104) : U=9834.5, p-value < 0.001
- July (n1 = 355) and April (n2 = 60) : U = 5940.5, p-value < 0.001
This has been added to the manuscript :

(l 333) *This difference appears significant at a statistical level. The Mann-Whitney U for the July and October cloud thickness distributions was 9834.5 (with sample sizes n1=355 and n2=104), yielding a p-value<0.001 (Mann and Whitney, 1947). The same is true for July and April (U= 5940.5, n1= 355 and n2= 60, p-value<0.001).*

l 287: "shoulder months": unclear, please do not use "shoulder months" throughout the manuscript and mention the months explicitly.
We agree that this expression is unclear and have removed it from the manuscript.

l 300: Again, how representative are the 222 profiles?
The calculation of S* from 222 profiles is not truly a scientific result of the paper, but more of a methodological point. Another option for calculating COD would have been to use a constant value of S* drawn from the literature. However, we felt it would be more robust to draw S* from our dataset itself, where possible. As it appeared that median S* values from our dataset vary substantially between months, we further felt that simply using the median value from the 222 profiles would bias the results, and so decided to use monthly S* values.

The object of this paragraph is to confront our values of S* with the literature, to check that they are within the enveloppe of expected values. As noted, we do not have any data about the microphysical composition of the clouds and so it is impossible to draw conclusions about the reasons for the variations of S*. This is why we have not looked further into the representativity of these 222 profiles. Such work would be interesting, but outside of the scope of this paper.

As noted before, we have decided not to include the March data in this paper. We have therefore deleted the following sentences, starting l. 311 :
« For example, the very high values observed in March [...] independent of other seasonal or temperature effect. »

Fig. 4. "a" and "b" missing in plot. Do you calculate the median and percentiles from e.g. 6 values? See for example March

« a » and « b » have been added to the plot, thank you for catching this. The median and percentiles for the lidar ratio are calculated from the points shown on the plot for each month. The March data is no longer included but the reviewer's point is applicable to April and November/December, which have less than 15 points each. As discussed above, we chose to use these monthly median values of S* for the calculation of COD despite the low number of points.

l 337 ff: I am not convinced that you can simply set the COD to 2 for high-IAB cloud layers. You simply do not know the COD in these cases. You state that this is helpful for examining the seasonal trend. But also this trend has large uncertainties then.
The reasoning for setting the COD at 2 for high-IAB cloud layers is the following :
- high-IAB cloud layers are, as a group, expected to have higher COD than low-IAB cloud layers ;
- low-IAB cloud layers have a 95th percentile value of 2
Therefore, for calculation of the median only, it makes some sense to set COD for high-IAB cloud layers to 2. In the median calculation, it ensures that the fact that high-IAB cloud layers exist, and are expected to have higher COD than low-IAB cloud layers, is accounted for.

The reviewer is correct that the ensuing trend is not certain. The alternative would be simply to set aside the high-IAB layers and treat only the low-IAB cases (this is the filled line in Fig. 4). But this would be akin to showing only half of the picture. We chose to show both calculations in order to avoid giving a false impression of the seasonal trend ; the peak in October appears robust, but the values in June (and generally in the summer) are quite probably larger than the values yielded by the low-IAB calculations.

We feel that this is a more rigorous presentation of our results. However, this was not explained in a clear way in the present manuscript. We have made the following changes :

(l 381) *To overcome this problem, the COD of high-IAB cloud layers was set to 2. This value was chosen as it is the 95th percentile of CODs calculated for low-IAB layers, and high-IAB cloud layers are as a group expected to have higher COD than low-IAB layers. The monthly median COD was then calculated including these high-IAB cases (Fig. 4, filled squares). This correction is not quantitatively robust as the value of 2 is arbitrarily chosen, not calculated. However, it accounts for the fact that high-IAB cloud layers exist, and are expected to have higher COD than low-IAB cloud layers, in the calculation of the median. This is helpful for examining the seasonal trend, which otherwise is biased by the presence of noise.*

It creates a significant difference in June and July, the months in which the percentage of high-IAB cloud layers is the highest. With this correction, the median monthly COD exhibits two peaks (June and October) and a minima in April. The October peak is however still the annual maximum, and does not appear to be strongly impacted by the inclusion of high-IAB cloud layers. Previous satellite measurements have exhibited a pattern of higher COD in spring and autumn, for instance May and October for the AVHRR data (Wang and Key, 2004) over the Arctic Ocean. The IAOOS dataset exhibits this October peak in single-layer COD. Another peak in June appears possible, although the IAOOS measurements are very uncertain in this month.

ll 382-383: Why was the information from the MPL not exploited as well?
The spirit of this study consists in extracting a multiyear statistic from the IAOOS database. Although the N-ICE2015 offers a more complete dataset than the IAOOS lidar from April – June 2015, it only covers three months of one year and does not therefore add meaningfully to the statistic.

The reviewer suggests using the MPL to check that the IAOOS lidar is able to reproduce its higher-resolution statistics. However, as stated in the general answer, we do not believe that such a case study would necessarily be representative.

l 389: "...due to the higher surface temperatures in spring/summer." Please elaborate on that.
This sentence is unclear and would indeed require more justification; for example, the impact of surface temperature on the downwards as well as the upwards flux. We have chosen to simplify it to the following observation:

(l 454) *[...] the netLW mode values are lower than in the winter. Indeed, both the downwards and upwards components of the longwave flux (LWd and LWu) increase from winter to summer. However, LWu increases more than LWd in both modes, causing a shift to lower netLW values.*

Fig.5 b) and c) Remove "Measured" in xlabel since also ERA5 data are shown. Explain RC1, RC2, OC in figure caption. Rather provide a detailed section on where the radiation sensors are installed in the text than mentioning it in the figure caption.
« Measured » has been removed. The caption now reads :

Panel a: time series of surface net longwave measurements during the N-ICE field experiment (second period, April-June 2015). The vertical lines indicate the time of IAOOS lidar profiles, with red lines corresponding to cloudless profiles. Panels b and c: histogram of the measured (filled line) and ERA5 (dashed line) net longwave flux during the N-ICE winter (b) and spring/summer (c) campaign periods. Panels d and e: hourly ERA5 vs measured net longwave in during the N-ICE winter (d) and spring/summer (e) campaign periods, with red dashed line indicating the 1:1 line. The colour corresponds to point density as calculated by a Gaussian kernel. For panel (e), three zones have been outlined. Zone "OC" contains points belonging to the opaquely cloudy mode of the measured netLW distribution. Zones "RC1" and "RC2" contain points belonging the radiatively clear mode of the distribution in April and May (RC1) and June (RC2).

The location of the buoy and the radiation sensors is now described in Sect. 2.2.1, as per our answer to one of the reviewer's previous comments.

l 404, Equation 5 What about the surface emissivity? Should be included in equation 5.
Thanks for catching this. The surface emissivity should indeed be included. Walden et al (2017) suggest a value of 0.99 is appropriate for the N-ICE campaign. The following line has been added below the equation:

(l 471) *[...] with epsilon the surface emissivity, which is assumed to be 0.99 (Walden et al., 2017).*

l 420: "...partly compensated by a 14 Wm-2 error in LWu in April/May..." Where can I see this? It would be interesting to include a plot of Lwu.
There is no plot of LWu in the paper as it stands. We discuss the relevant findings as to LWu and LWd in the text, for example in this sentence. Although a more detailed discussion of the upwards and downwards components of the flux would be interesting, perhaps they would best belong to another paper, focusing specifically on ERA5.

Figure 6: Please use different line styles for the different cloud optical depth. Remove "Evolution" from figure caption: "Longwave downward radiative flux as a function of..."
The suggested changes have been made.

ll 425: Which kind of satellite data are assimilated in ERA5 exactly? Please provide more details here which underline your hypothesis.
Infrared and microwave radiances from several different satellites are assimilated in ERA5. This includes measurements of cloud liquid water from the AMSR-2 instrument aboard GCOM-W1, AMSR-E aboard AQUA, GMI aboard the GPM Core Observatory, and others (see the ECMWF website : https://confluence.ecmwf.int/pages/viewpage.action?pageId=82870405#ERA5:datadocumentation-Table14)

However, we have decided to remove this hypothesis as it was not formulated on sufficiently solid grounds. ll. 425 to the end of the paragraph (in the original manuscript) has been replaced with a simple observation:

(l 492) *More investigation is required as to the ultimate source of this error.*

ll 441 ff: It is totally unclear why you need to come up with parameterizations or estimates of the downward radiative flux components. These are measured, aren't they? What is the intention of this part?
The goal of the parametrisation was to help discuss the impact of COD, SZA, and surface temperature on the downwards surface fluxes. This is mainly important for COD, which was not measured explicitely during SHEBA. It is also helpful for discussing the cloud net radiative forcing beyond the N-ICE campaign. This last part has been expanded in the modified manuscript as a response to the comments below.

l 473: "shortwave cloud albedo effect"
The suggested change has been made.

ll 476-478: "In contrast, the longwave warming effect, ..." Maybe it would be good to remind the reader that this is the difference between the dashed and solid line in Fig.6 (as far as I understood).
The reviewer's understanding is correct – and the suggested clarification is likely a good idea. The sentence has been edited to :

(l 544) *In contrast, the longwave warming effect (i.e., the difference between the dashed/dotted and solid lines in Fig. 6a) varies little [...]*

ll 482-484: "This explains that . . ." Can you elaborate on that a little bit more? Unclear to me.
We decided that this point would be best adressed in a new section (Sect. 5.4 « Beyond NICE2015 : estimating the summer cloud net radiative forcing at the surface » in the revised manuscript, **l 554 - 599**), in which we calculate and plot the net cloud radiative forcing directly.

ll 489-491: "Equations 6 and 7 were inverted to calculate . . ." Can you explain in detail how you did it? In Eq. 7, COD is not directly included. It might be good to remindthe reader how this is connected to transmittance. Do you take F0 from your fitted function?
In Eq. 7, LWd is calculated using
1) F_0 , which we fitted from the data and depends only on solar zenith angle;
2) T_c , which is calculated using the parametrisation of Fitzpatrick et al., 2003.
The parametrisation of T_c depends on solar zenith angle (theta), surface (albedo) alpha, and COD. For given values of theta, alpha and LWd we were therefore able to compute COD using a numerical equation solver (fsolve from the scipy.optimize package in python). We chose not to explicitely write out the parametrisation of Fitzpatrick in our paper because it is quite unwieldy, however every detail is in the referenced article.

Section 4.4 was moved to supplementary materials (Appendix B) in order to streamline the structure of the paper. However, we made the following modification :

(l 674) *Equations 6 and 7 were inverted* ***using a numerical equation solver*** *to calculate [...]*

Table 4: What are the uncertainties of the derived COD values?
There are three different sources of uncertainty for the derived COD values: a numerical uncertainty (from the solver), an uncertainty linked to the input parameter error (temperature, SWd, albedo and LWd), and the uncertainty due to the model itself. The first is expected to be small. The third is large but somewhat besides the point, as the aim here is specifically to compare IAOOS CODs to those obtained from inverting these models. Therefore we chose to focus on the second.

For tau_SW, the error ranged 8 % to 19 % (mean 11%). This was calculated by a Monte Carlo method. We drew 100 random values of albedo and SWd from the following distributions :
- for albedo : a normal distribution centered on 0.8 with a standard deviation of 0.025, therefore respecting the spread of actual measured albedos during N-ICE2015 (0.75 – 0.85);
- for SWd : a normal distribution centered on each measured SWd value and with a standard deviation equal to half the measurement error. This is the maximum of 3 % of the measured value and 5 W m^{-2} (see presentation of the N-ICE measurements).

For tau_LW, the error ranged from 9 % to 23% (mean 13%). This was also calculated with a Monte Carlo method. 100 random values of temperature and LWd were drawn from the following distributions :
- for temperature : a normal distribution centered on each measured temperature value and with a standard deviation equal to half the measurement error. This is the maximum of 2.4 % of the measured value and 0.3°C (see presentation of the N-ICE measurements).
- for LWd : same as above, the measurement error is the maximum of 2 % of the measured value and 3 W m^{-2}.

In both cases, the error was then calculated as the mean absolute percentage error of the result over these 100 points.

This was specified in the caption to Table B1 :
Individual errors carried over from measurement errors on LWd, SWd and T2m are in the range 8−22% (mean 14%) for τ_{SW}, and 10−30% (mean 15%) for τ_{LW}.

And in the text:
(l 674) *Equations 6 and 7 were inverted using a numerical equation solver to calculate the broadband shortwave and longwave CODs τ_{SW} and τ_{LW} from the N-ICE SWd, LWd and temperature values at the time of the IAOOS profiles. Albedo was taken as fixed and equal to 0.8 in this calculation. The measurement errors of SWd, LWd and temperature (Sect. 2.2.1) as well as the choice of a fixed albedo create an error on τ_{SW} and τ_{LW} which is estimated through a Monte Carlo method. This error is no more than 19% for τ_{SW} and 23% for τ_{LW} (Table B1).*

ll 521-522 and this section: “The results show a significant seasonal variation . . .”. Overstated due to the reasons mentioned before. Also “Monthly cloud frequency is minimum in March/April and November/December . . .” A discussion of measurement and sampling uncertainties is needed here! I doubt that the results a robust for these months.

This has been reworded :

(l 607) *The low number of profiles in some months causes some uncertainty on specific monthly cloud properties. However, the results show statistically significant differences in cloud cover and optical and geometrical properties of clouds between the summer and April, November and December.*

Reply to RC2

Global comment
Arctic low clouds are a key climate feature of the atmospheric boundary layer over the Arctic Ocean. Arctic low clouds are important because of their strong influence on the amount of solar and infrared radiation that is incident on the surface. In the meantime, they can strongly modify the low-level heat, moisture and momentum fluxes. This paper quantified the seasonality and surface radiative impacts of Arctic low clouds from the Ice, Atmosphere, Arctic Ocean Observing System (IAOOS) field campaign. It is a very important topic as the Arctic is a data-sparse region. Moreover, both passive and active remote sensing products have their limitations on polar cloud retrievals. Therefore, the information obtained from this five-year campaign is very valuable. Overall, this paper is well written, but the structure needs to be improved. I recommend it to be accepted after following issues being addressed. Please find my specific concern as below.

We would like to thank the referee for the positive appreciation of our work and for the helpful suggestions below as to the structure.

Specific comments
Overall: The current version contains too much information. I find it a bit difficult to follow because of the paper's structure, which is not well organized and logical. The section 4.1.4 is tightly connected with section 4.3. The author also mentioned that "The reasons for this are explored in Sect. 4.3 by investigating the summer radiative balance." (line 362-363). Is it better to combine these two sections together? From my perspective, a better structure would be the seasonality of cloud properties, impact of cloud on surface temperature and radiation budget, and followed by the comparison of ERA5 to surface in-situ measurements. And I am quite sure how to combine section 4.4 with other sections. Also, I believe the authors need to add transitional sentences and paragraphs to connect these sections in a more logical way.

We agree that the paper has quite a complex structure, which might lead to confusion. We decided to take the reviewer's comment into account to make the paper's logical progression clearer.
- Sections 1, 2, 3 are unchanged
- Section 4 has been changed to « Seasonality of Arctic low clouds properties during IAOOS», covering the previous sections 4.1.1, 4.1.2, 4.1.3
- A new section 5, « Cloud impact on surface temperatures and radiative balance», covers previous sections 4.1.4, 4.2 and 4.3.
- A new section 5.4 « Beyond N-ICE2015: estimating the summer cloud net radiative forcing at the surface » was added discussing the cloud net radiative forcing in the summer.
- Section 4.4 has been moved to the appendix (Appendix B)
However, the section concerning ERA5 was kept just after the analysis of the two radiative modes. This is because it is not a global comparison of ERA5 to surface in-situ measurements over the course of the compaign, but a short evaluation of the

representation of these modes in ERA5. We therefore feel that it makes more sense to keep these two sections in close connection.

The introduction has been updated to make the logical progression of the paper clearer, and we have added more transitional sentences (especially in Section 5). For example, at the end of Section 5.1 :

(l 396) *In the following sections, we look at the summer surface radiative balance in order to gain a better understanding of the mechanisms behind this seasonal variation in temperature difference between cloudy and cloudless profiles. First, the link between the net surface longwave flux and the presence of clouds is investigated (Sect. 5.2.1) from compared N-ICE and IAOOS measurements. Then, the influence of other factors such as solar zenith angle, temperature and COD on downwards shortwave and longwave fluxes during the N-ICE2015 April to June period is explored (Sect. 5.3). Lastly, the discussion of the net cloud radiative forcing at the surface is extended to the months of July and August using a simple parametrisation (Sect. 5.4)*

See also the beginning of Sect. 5.3 :
(l 494) *In the Arctic summer, clouds impact the surface radiative budget in two competing ways: they have a longwave warming effect and a shortwave cooling effect. In Sect. 5.2.1, the N-ICE2015 April-June netLW distribution was shown to be bimodal, withthe first mode corresponding to the presence of clouds in the IAOOS profiles and the second to their absence. However, other factors than the absence or presence of clouds may impact the surface radiative fluxes, both shortwave and longwave. In this section, the influence of variables such as the solar zenith angle, COD and surface temperature on the downwards fluxes (both longwave and shortwave) from the N-ICE2015 April-June period is explored and parametrisations of these fluxes are introduced.*

Line 5-6: “Cloud frequency is globally at 75%, and above 85% from May to October.” Why the cloud frequency is globally? Not in the Arctic?
« Globally » here means the April – December average over the whole campaign period. The text has been edited to make this clearer and now reads :

(l 5) *The average cloud frequency from April to December over the course of the campaign was 75%. Cloud occurrence frequencies were above 85% from May to October.*

Line 59-60: I think you could also mention that CALIPSO satellite product has limitation on temporal coverage, which is only available after 2006.
This has been added, thank you for the suggestion.

(l 62) *Their record is also more limited in time than that of ground-based stations (from 2006 for CALIPSO)*

Figure 4: There are no (a) and (b) in the figures.
Thank you for catching this, it has been fixed.

Section 4.1.4 and Table 3: How many cloudy and cloudless profiles are there for each moth? For example, you may rarely get cloudless profiles in summer as low cloud frequency is pretty high. Does this issue affect your results?
The total number of profiles is indicated in Tables 2 and 3 ; we have not included the number of cloudy profiles in these tables but they can be calculated using the cloud fraction (which is indicated). The issue of the reliability of the statistics due to the low number of profiles in some months was raised in detail by the other referee, and we have decided to introduce confidence intervals to make the discussion of the results

more rigorous (see new Sect. 4.1). In light of these intervals we do not believe that the number of profiles affects our main point – which is that there is a statistically significant seasonal variability in cloud occurrence frequency. Please note that we have decided to restrict ourselves to months with more than 30 profiles, as this is the usual rule of thumb in statistics. All references to March statistics have therefore been deleted from the text.

See **ll 266** onwards in the revised manuscript :
The results of IAOOS dataset are shown in Table 3 and Fig. 2. Note here that the number of profiles available for each month is variable, both because of the more favorable operation conditions in the summer and the timing of the buoy deployment (usually in May). As such, there are more than 200 profiles from May to September, around 100 in April and October, and less than 54 in November and December. Months with less than 30 profiles, i.e. January, February, and March, are not treated in this article. Care must therefore be taken in analysing the results of late autumn and winter. A 90% confidence interval for the cloud occurrence frequency can be estimated from a Bayesian calculation, assuming that the number of cloudy profiles followsa binomial distribution and supposing an appropriate a priori distribution for the cloud frequency from the literature (Appendix A).

The IAOOS data shows a similar trend as the literature, with generally higher cloud cover values. From May to October, clouds are present over 85% of the time (Fig. 2). In contrast to the previous ground-based climatologies outlined above, there are two peaks at more than 0.9 in the monthly cloud frequency, although they differ little from the summer baseline. The first is in June, which has a mean cloud frequency of 0.92 and a confidence interval of (0.88−0.94). The second peak is in October, also with a mean cloud frequency of 0.92 but with a slightly wider confidence interval (0.85−0.95) because of the lower number of profiles. This is reminiscent of the results of Zygmuntowska et al. (2012), from CALIPSO data, which show a peak in cloud occurrence above 0.9 in October. July and August have slightly lower cloud frequency values (0.85 (0.82−0.88) and 0.85 (0.8−0.89) respectively). However, since there is non negligible overlap between the confidence intervals of June/October and the other summer months, it is difficult to draw solid conclusions as to May - October variability.

In the IAOOS dataset, April and November appear to mark a sharp transition in cloud occurrence frequency from the summer values. April has a cloud frequency of 0.59 (0.52−0.67) while the cloud frequency in November is 0.56 (0.48−0.68). While the confidence intervals are quite wide here due to the lower number of profiles, there is no overlap with the summer confidence intervals. This suggests that the lower cloud frequencies observed during the months of April and November is meaningfully different from that of the months of May through October. December cloud frequency is lower still, at 0.32 (0.29−0.51). Note however the width of the confidence interval and the fact that the December data corresponds to a single year of measurement (2017).

Section 4.1.4: The clear-sky LW flux also exerts large influence on surface temperature. In most of cases, the magnitude of clear-sky LW flux is larger than that of cloud longwave radiative effect. We usually believe that the high pressure tends to reduce clouds and associated cloud warming effect. However, the high pressure in the upper troposphere could also increase the clear-sky LW flux and enhance surface warming. In addition, the authors tried to investigate the impacts of clouds on surface temperature by using lidar profiles with and without low clouds. Then how to make sure other conditions (e.g. large-scale circulation) remain same between two groups? I understand that this may not easy to be addressed. But authors should treat this issue more carefully.

Reference:
Ding, Q., Schweiger, A., L'Heureux, M., Battisti, D. S., Po-Chedley, S., Johnson, N. C., ... & Steig, E. J. (2017). Influence of high-latitude atmospheric circulation changes on summertime Arctic sea ice. Nature Climate Change, 7(4), 289-295.

If we understand correctly, the reviewer's argument is the following :
- The downwards longwave flux (LWd) is the sum of a clear sky component (LWd_{cs}) and of a clouds component (LWd_{cl}) – if clouds are present.
- LWd_{cs} is expected to vary according to synoptic conditions. In particular, high pressures (in the upper levels of the troposphere) are associated with subsidence, warming the troposphere and therefore increasing LWd_{cs} (Ding et al, 2017.)
- High pressures (at which level?) are also associated with less clouds.
- The magnitude of variation of LWd_{cs} is comparable or larger than the cloud longwave radiative effect (LWd_{cl}).
- Therefore, total LWd becomes :
    - LWd = $LWd_{cs}(1)$ under high pressures (no cloud effect, high LWd_{cs})
    - LWd = $LWd_{cs}(2)$ + LWd_{cl} under low pressures (clouds, but low LWd_{cs})

and ($LWd_{cs}(1)$ – $LWd_{cs}(2)$) ~ LWd_{cl}, which means that there is little total difference between LWd under high pressures (cloudless conditions) and low pressures (cloudy conditions).
Therefore, the absence of an observed surface temperature difference between cloudy and cloudless profiles could simply be due to a compensating effect in clear sky LWd.

This is an interesting and valid point. As a first remark, this mechanism would also be expected to hold true in autumn and spring : however, we do observe a significant surface temperature difference between cloudy and cloudless profiles in these seasons. Secondly, this is only schematic. The different variables and their variations would need to be quantified. For example, at what frequency do clouds occur under high and low pressure respectively ? (For that matter, is the confounding variable surface pressure or geopotential in the higher levels of the troposphere?) What is the magnitude of variation of LWd_{cs} in comparison with LWd_{cl} ? Without these informations, it is hard to tell if the proposed effect would be significant or not.

While Ding et al (2017) establish a link between increased geopotential at 200 hPa and increased LWd and temperature at the surface, they do not distinguish between clear sky and cloud LWd. In contradiction with the proposed mechanism above, they show that higher geopotential at 200 hPa is linked to a decrease in mid and high-level clouds and a slight increase in low-level cloudiness over the central Arctic Ocean. They judge this to be consistent with the observed augmentation in LWd.
It is not clear therefore that the above mechanism would be valid, as « higher pressures » (i.e. higher geopotentials at 200 hPa) are not associated with less clouds.

However, it is true that large-scale circulation is an important parameter that we fail to control for. As pointed out by the reviewer and outlined above, a true treatment of this issue would be complex and out of the scope of this paper.
Some elements of an answer are below.
The IAOOS buoys were equipped with barometers as well as temperature sensors. It appears that surface pressures for « cloudy » and « cloudless » profiles are not different at a statistically significant level except in August and November. In both of these months, the lidar profiles that contain clouds appear to coincide with markedly higher surface pressures than those that don't contain clouds (+12 hPa). However, there is a strong temperature difference in November but not in August. In all other summer months cloudy and cloudless profiles appear to have similar surface pressures. In short the two groups do not appear to sample wildly different conditions.

This has been clarified in the manuscript.

(l 407) *As noted before, louds are naturally not the only factor impacting surface temperatures or even the downwards longwaver adiative flux. Large-scale circulation is also important: for example, high geopotential at 200hPa is linked to a warming of the troposphere through subsidence, which increases the longwave radiative flux received at the surface (Ding et al., 2017). It is therefore important to check that cloudy and cloudless lidar profiles do not sample different surface pressures. The IAOOS buoys were equipped with barometers as well as temperature sensors. It appears that surface pressures for cloudy and cloudless profiles are not different at a statistically significant level, with the exception of August and November. In both of these months, the lidar profiles that contain clouds appear to coincide with markedly higher surface pressures than thosethat don't contain clouds (+12 hPa, Mann-Whitney test p-values <0.005). As surface temperatures in the two groupes differ strongly in November but not in August, however, surface pressure does not appear to be a confounding factor for surface temperature and cloud occurrence.*

Line 425: "This may ultimately be due to an error in the satellite data that is assimilated by the ERA5 reanalyses." Which satellite data is assimilated by the ERA5? Can you be more specific about this bias?
Infrared and microwave radiances from several different satellites are assimilated in ERA5. This includes measurements of cloud liquid water from the AMSR-2 instrument aboard GCOM-W1, AMSR-E aboard AQUA, GMI aboard the GPM Core Observatory, and others (see the ECMWF website : https://confluence.ecmwf.int/pages/viewpage.action?pageId=82870405#ERA5:datadocumentation-Table14)

However, we have decided to remove this hypothesis as it was not formulated on sufficiently solid grounds. ll. 425 to the end of the paragraph has been replaced with a simple observation:

(l 492) *More investigation is required as to the ultimate source of this error.*

Line 464-467: Is N-ICE second period from April to June? Since you used a fixed surface albedo 0.8, which excludes the impacts of reduced multiple reflections between surface and clouds with sea ice melt, particularly from April to June. Can you comment on that?
Yes, the second period is from April to June. We used a fixed albedo of 0.8 because in practice, the measured albedo during the N-ICE April-June period varied only from 0.75 – 0.84, which doesn't change the LWd much using the Fitzpatrick parametrisation. For example, for a solar zenith angle of 55° and a cloud optical depth of 20, the difference in LWd between an albedo of 0.75 and 0.8 is only 7 %. As our model is mainly illustrative, this is an acceptable error.

Line 480: "This translates into a total shortwave cloud forcing that ranges between −20 to −60 W m −2 , assuming an albedo of 0.8." Again, I believe that surface albedo plays an important role in determining the shortwave flux at the surface. Assuming a surface albedo of 0.8 could totally ignore the multiple reflections between clouds and melting surface.

Reference:
Wendler, G., Moore, B., Hartmann, B., Stuefer, M., & Flint, R. (2004). Effects of multiple reflection and albedo on the net radiation in the pack ice zones of Antarctica. Journal of Geophysical Research: Atmospheres, 109(D6).

We agree with the reviewer that the albedo impacts the shortwave flux quite consequently. The assumption is only in regards to the N-ICE dataset, for which the

albedo did not vary much from a value in 0.8. The following phrase has been added for clarification:

(l 549) *[...] assuming an albedo of 0.8* ***(typical of the N-ICE campaign April-June period)***

Please note that in response to this comment and another comment made by the first reviewer, we have decided to add a new Section 5.4. « Beyond NICE2015 : estimating the summer cloud net radiative forcing at the surface » which explores the impact of albedos on this parametrisation.

Line 522: “Low cloud cover (i.e., with a base beneath 2 km) is found to be 76% globally over the course of the campaign.” What it is globally?
This has been modified to

(l 609) *averaged over all months of the campaign*

for more clarity.

Characterisation and surface radiative impact of Arctic low clouds from the IAOOS field experiment

Julia Maillard[1], François Ravetta[1], Jean-Christophe Raut[1], Vincent Mariage[1], and Jacques Pelon[1]

[1]LATMOS/IPSL, Sorbonne Université, UVSQ, CNRS, Paris, France

Correspondence: Julia Maillard (julia.maillard@latmos.ipsl.fr)

Abstract. The Ice, Atmosphere, Arctic Ocean Observing System (IAOOS) field experiment took place from 2014 to 2019. Over this period, more than 20 instrumented buoys were deployed at the North Pole. Once locked into the ice, the buoys drifted for periods of a month to more than a year. Some of these buoys were equipped with 808 nm wavelength lidars which acquired a total of ~~1805~~ 1777 profiles over the course of the campaign. This IAOOS lidar dataset is exploited to establish a novel statistic of cloud cover and of the geometrical and optical characteristics of the lowest cloud layer. ~~Cloud frequency is globally at~~ The average cloud frequency from April to December over the course of the campaign was 75%~~, and~~. Cloud occurrence frequencies were above 85% from May to October. Single layers are thickest in October/November and thinnest in the summer. Meanwhile, their optical depth is maximum in October. On the whole, the cloud ~~cover~~ base height is very low, with the great majority of first layer bases beneath 120 m. In ~~the shoulder seasons~~April and October, surface temperatures are markedly warmer when the IAOOS profile contains at least one low cloud than when it does not. This temperature difference is statistically insignificant in the summer months. Indeed, summer clouds have a shortwave cooling effect which can reach -60 W m^{-2} and balance out their longwave warming effect.

1 Introduction

The Arctic is a key region of climate change: it is warming about twice as fast as the middle latitudes. This phenomenon, called "Arctic amplification", is most commonly attributed to the ice-albedo feedback, which is due to areas of open ocean exposed by melting sea ice absorbing more solar radiation. However some models with fixed albedos also appear to show amplified warming in the Arctic, pointing to other mechanisms at work (Winton, 2006; Pithan and Mauritsen, 2014). Clouds are one of the main contributors to uncertainty in global climate models because cloud feedbacks and cloud-aerosol interactions are still poorly understood; however, clouds appear to be of particular importance in the Arctic (Tjernström et al., 2008), where they play a very important role in the climate system. Indeed, Arctic clouds are observed to influence the melting of sea ice (Kay and Gettelman, 2009) and may exert control on the ice-albedo feedback this way. However, these effects and processes are seasonally variable and not well represented by annual means (Kay and Gettelman, 2009).

Firstly, the cloud cover in the Arctic has a large seasonal variability: it is especially extensive in the summer and reaches a minimum in the winter (Curry et al., 1988, 1996). This result is well attested in the literature although values and trends tend to differ between studies and instruments. For example, during the Surface Heat Balance of the Arctic (SHEBA) campaign, winter

cloud occurrence measured from a combined radar/lidar was 70%. It increased to over 80% in the summer months and reached a 95% peak in September (Shupe et al., 2006). Using data from CALIPSO (Cloud-Aerosol Lidar and Infrared Pathfinder Satellite Observations), Zygmuntowska et al. (2012) find two peaks of 85% and 90% in May and October respectively, and a minimum in January-March around 70%, in good agreement with Shupe et al. (2006). However, in the same study, cloud fractions retrieved from the space-borne Advanced Very-High-Resolution Radiometer (AVHRR) instrument were $< 60\%$ for the whole October-April period, and never rose above 80%.

Cloud microphysical characteristics and radiative impact are also seasonally-dependant. Winter clouds contain mostly ice and are therefore less emissive than summer liquid-containing clouds, although mixed-phased clouds maintain themselves throughout the year (Morrison et al., 2011). However, seasonal statistics of cloud optical depth (COD) over the Arctic ocean are scarce and uncertain: based on the AVHRR radiometer data for example, Wang and Key (2004) found a slight seasonal variation in the cloud optical depth over the Arctic ocean, with a peak in May and October (> 6) and lower values (≈ 5) in the winter. It has been shown that cloud radiative forcing is positive (i.e., clouds warm the surface) for much of the year, except for a short period in late June to early July when the cloud shortwave forcing is larger than the longwave forcing (Intrieri et al., 2002a). Indeed, in contrast to winter, clouds impact the surface radiative budget in two competing ways in the summer. As in winter, they provide longwave warming; but they also have a shortwave cooling effect, by preventing solar radiation from reaching the surface.

Large uncertainties remain about the characteristics of Arctic clouds and their surface impact, in part because more data and observations are needed (Kay et al., 2016). Ground-based measurements are sparse in the Arctic because of the harsh conditions and the lack of permanent settlements. The ground-based measurement stations of the International Arctic Systems for Observing the Atmosphere (IASOA) network (Uttal et al., 2016), for example Eureka (Nunavut, Canada) or Barrow (Alaska) are necessarily coastal. Nevertheless, ground-based stations have continuous data coverage with a record covering several years, and have therefore given precious information on Arctic clouds and their properties (Shupe et al., 2011; Nomokonova et al., 2019). Measurements on the sea-ice take the form of ship-based or airborne campaigns, covering only a narrow spatial and temporal window. The first such campaign was SHEBA, which covered a full year from October 1997 to October 1998. Although it yielded significant results (Stramler et al., 2011; Shupe et al., 2006), it is now more than 20 years old and not representative of the modern Arctic. Subsequent campaigns aimed at studying the Arctic's changing conditions such as the Arctic Summer Cloud Ocean Study (ASCOS) (Tjernström et al., 2014), the ACLOUD/PASCAL campaign (Wendisch et al., 2019), the Arctic Clouds in Summer Experiment (ASCE) (Sotiropoulou et al., 2016) or the Norwegian Young Sea Ice Experiment (N-ICE) (Walden et al.) covered one to six months, disproportionately in the summer. Most recently, the Multidisciplinary drifting Observatory for the Study of Arctic Climate (MOSAiC) campaign is a one year-long study of the Arctic climate, with clouds as one of many research axes. The drift is due to end in September 2020.

In this context, many established statistics - e.g., Wang and Key (2004) - make use of satellite measurements, which have large coverage but are flawed at high latitudes. Indeed, spectroradiometers (such as MODIS, or the AVHRR) may have difficulties in distinguishing clouds from the underlying sea-ice. Their performance also differs between the dark winter months and the summer (Zygmuntowska et al., 2012). All in all, there are large differences in measured values between instruments

(Chan and Comiso, 2013). Satellite-based lidars such as the instrument aboard CALIPSO give more reliable measurements but are limited to 82°N because of the satellite flight path (Winker et al., 2009). Their record is also more limited in time than that of ground-based stations (from 2006 for CALIPSO).

This paper presents results of the Ice, Atmosphere, Arctic Ocean Observing System (IAOOS) field experiment lidar measurements. This novel database offers a ground-based view of lower tropospheric clouds at very high latitudes (over 80°N) over a significant period of time - from 2014 to 2019 (Mariage, 2015). A small part of this dataset has already been analysed in Di Biagio et al. (2018) and Mariage et al. (2017). Here it is treated as a whole to extract a ~~5~~ multi year statistic of the ~~Arctic cloud cover~~ April to December cloud cover along the track of the drifting buoys. First, the IAOOS field campaign and other relevant datasets are presented (Sect. 2). Then the treatment of the IAOOS lidar data and the derivation of cloud characteristics are explained (Sect. 3). The obtained statistics of cloud frequency, and geometrical and optical properties are presented in Sect. ~~4.1 and~~ 4. Finally the impact of ~~the~~ clouds on surface ~~radiation and temperature is explored in Sect. 4.2 and 4.3~~temperatures and radiative balance is explored (Sect. 5).

2 Data used

2.1 The IAOOS field campaign: a 5 year study of the Arctic troposphere

2.1.1 Deployed instruments

The IAOOS field experiment was led by Sorbonne University - through the LATMOS and LOCEAN laboratories - with the support of several structures, among which the French polar institute IPEV (Institut polaire français Paul-Emile Victor) and the technical division of the Institute for Earth Sciences and Astronomy (CNRS-INSU) from 2014 to 2019. The main campaign objective was to "collect real time observations of the ocean, ice, snow and atmosphere of the Arctic", offering a complementary viewpoint to that of satellites (L2). In order to do this, several instruments were installed on an autonomous floating platform (or buoy). These buoys were then locked into the pack ice and left to drift with it for a duration of several months to a year. During that time period, the buoys were tracked by GPS and communicated the acquired data to the IPEV office in Brest (48°23′24″ N, 4°29′24″ W) every day.

The main instrument on the "atmosphere" side of the buoys was a micro lidar, which was was designed to study lower troposphere and has a clear-sky range of around 4.4 km in the daytime, and 13.7 km at night, with a vertical resolution of 15 m (Mariage, 2015; Mariage et al., 2017). The wavelength was chosen in the near infrared (808 nm) in order to avoid disturbing the local fauna while maintaining a distinct molecular signal. This is similar to many commercial ceilometers (Mariage, 2015). However, it had to be custom made to resist the tough Arctic conditions. Indeed, several key components of a lidar are sensitive to ambient temperature variations, and the buoys' operating conditions in the pack ice could be up to 40°C colder than the lab where it was calibrated. The lidar therefore had to be modified and isolated in order to keep it at a near constant temperature (Mariage, 2015). Furthermore, the tube containing the lidar emitter and receiver was topped with a window that, in operating conditions, was often covered by frost. This layer of frost attenuates the signal, and, in extreme cases, totally blinds the lidar.

Buoy	Start date	End date	Nb of exploitable profiles
B02	13/04/2013	02/12/2014	462
B12	26/04/2015	05/06/2015	73
B24	06/04/2017	20/11/2017	322
B25	15/08/2017	28/10/2018	429
B27	19/04/2018	17/03/2019	~~519~~ 491

Table 1. Start and end date of the buoy lidar data acquisition and number of exploitable profiles. Note that buoy B07 also yielded some profiles (Di Biagio et al., 2018) which are not treated here.

In order to overcome this problem a window heating system was put in place. The actual heating was limited to the 10-minute interval before the two- to four-time daily profile acquisition in order to avoid draining the battery too fast. Theoretically, this ensured that the lidar window was clear during measurement. However, in practice, the frost prevented lidar measurements from mid-December to early March. The frost problem will be further detailed in Sect. 3.1.1.

The buoys were also equipped with temperature and pressure sensors for measuring outside conditions; and internal temperature and humidity sensors for monitoring the lidar system. On the underwater portion of the buoys, a float measured ocean temperature and salinity while an Ice Mass Balance system acquired temperature profiles of the snow, ice and liquid water layers - see Koenig et al. (2016).

2.1.2 Buoys and tracks

The first IAOOS platform was deployed in 2013. Since then, more than 20 buoys have drifted in the Arctic pack ice, and the last one was deployed in August 2019. However, not all buoys were equipped with lidars and not all deployed lidars operated successfully. In particular, the data transmission system of the 2016 buoys functioned poorly, and there are no exploitable lidar profiles from July 2015 to March 2017 (see Table 1). All in all, five buoys yielded usable lidar data, amounting to ~~1805~~ 1777 profiles covering the ~~March~~ April to December months. A vast majority of the drift took place north of 82°N (red ~~line~~circle, Fig. 1). Furthermore, apart from one buoy, all trajectories were confined to the Atlantic sector of the Arctic, reflecting the transpolar drift stream. Indeed, most buoys studied here were locked into the ice close to the North Pole.

2.2 Other data

2.2.1 N-ICE

~~Four IAOOS buoys were deployed during the~~ The Norwegian Young Sea Ice Experiment (N-ICE) campaign ~~, which~~ took place from January to June 2015. During that time, the research vessel Lance drifted with four different ice floes (Walden et al.; Cohen et al., 2017

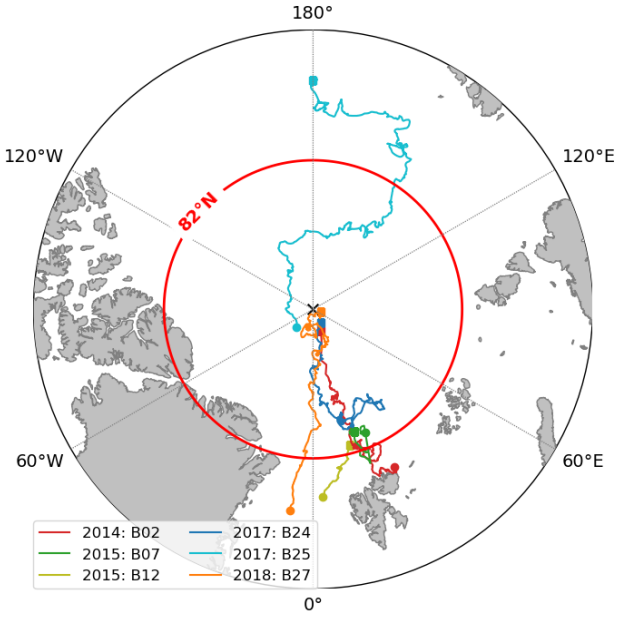

Figure 1. Map of the IAOOS buoy tracks, 2014-2019 (this map only includes buoys which delivered the lidar data exploited in this article). The different colours correspond to the different buoys, with the year of launch indicated. The red circle corresponds to the 82°N latitude: north of this circle, no satellite lidar data is available.

. The first two drifts took place during the winter (January - March 2015~~aboard the R/V Lance research vessel (Walden et al.). The buoys drifted in the sea-ice close to~~) while the last two drifts occurred in the late spring to early summer period (April to June 2015). On each floe, a "Supersite" ice camp was installed about 300 m away from the research vessel. ~~The goal of this field campaign was to investigate thin, first-year sea-ice and its interactions with the rest of the Arctic system; instruments deployed included an MicroPulse Lidar (MPL) to determine cloud phase and a four component radiometer. Radiosondes were also~~ Atmospheric measurements were mostly performed at this Supersite. Surface longwave fluxes (up and down) were measured with a Kipp & Zonen CGR4 pyrgeometer, which has a 4.5 to 42 μm bandwith. The shortwave fluxes (up and down) were measured with a Kipp & Zonen CMP22 pyranometer (200 to 3600 nm bandwidth). Both these instruments were heated and ventilated using a Kipp & Zonen CVF4 unit. Their accuracy is 3% (or 5 W m^{-2}) for the shortwave, and 2% (or 3 W m^{-2}) for the longwave (Walden et al., 2017; Hudson et al., 2016). The temperature at two meters was measured with a ventilated and shielded Vaisala HMP-155A sensor which has an accuracy of 2.4% (or 0.3°C) (Graham et al., 2017; Cohen et al., 2017). In addition, radiosondes were launched twice-daily from the research vessel, yielding profiles of relative humidity, temperature and wind speed ~~. The radiative flux and meteorological data from the second period (April to June) of this campaign were in this study~~ (Walden et al., 2017).

Four IAOOS buoys were deployed during this campaign and drifted in the ice floe close to the research vessel. In particular, the B12 buoy was locked into the third ice floe 200m away from the Supersite from end of April to the beginning of June

2015 (Fig. 1). Because of the proximity of the buoy to the Supersite over this period, the N-ICE surface radiative flux and temperature measurements can be used as a complement to the IAOOS data~~(see~~. This allowed us to evaluate the radiative impact of clouds on the surface in late spring to early summer (Sect. 5.2.1 and 5.3).

2.2.2 ERA5

ERA5 is the new reanalysis from the European Center for Medium-Range Weather Forecast, replacing ERA-Interim (Hersbach et al., 2020) . ERA5 provides hourly or four times daily estimates of many weather variables on a 0.25°x0.25° grid and with 137 vertical levels. It is made available online with a three month delay ~~(L1)~~(Copernicus Climate Change Service (C3S), 2017). Here we interpolated the ERA5 values on the IAOOS positions using bilinear interpolation in space (and linear interpolation in time) during the N-ICE drift period. This allowed us to compare the radiative flux values measured during N-ICE with the ERA5 reanalyses (see Sect. 5.2.1).

3 Methodology of the IAOOS lidar data treatment

3.1 Overcoming Arctic-specific challenges

3.1.1 Lidar window frost

Several problems are associated with the autonomous drift of a lidar in harsh Arctic conditions, as outlined in Sect. 2.1. In particular, the cold conditions cause frost to form on the lidar window, because the installed window heating system could not operate the whole time in order to preserve batteries. This caused the signal to be attenuated and therefore the system constant C - which is the ratio of the raw signal in photon numbers to the actual signal - to diminish.

Because it is crucial to know the system constant value in order to extract geophysical information from the raw lidar signal, this effect had to be corrected. The correction method was put in place by Mariage (2015). First a "frost index", γ is defined:

$$\gamma = \frac{P_0}{P}$$

where P is the lidar window reflection peak, and P_0 the minimal value taken by P over the course of a drift. P_0 is therefore assumed to be the value of the reflection peak when the window is entirely frost-free. γ then ranges from approximately 1 when the window is frost free to very low values ($< 5 \cdot 10^{-2}$) when the window is totally opaque. In fact, this frost index becomes a proxy for the window transmittance.

Under the assumption that aerosol load is very low in the high Arctic, C can be calculated from cloud-free profiles. Its values are then compared to the frost index. As could be expected, $\frac{1}{C}$ diminishes with γ: that is, the signal is dampened when the window is covered with frost. An empirical fit of $\frac{1}{C}$ as a function of γ can then be established (Mariage, 2015). This allows us to deduce the value of C for each profile from the value of γ. The fitting coefficients were determined independently for each buoy when possible, since the frost index depends on P_0, which is buoy specific.

It should be noted however that when the frost is too thick ($\gamma \leq 0.05$), no usable signal is recoverable. This means that there were no exploitable lidar profiles in late December to early March. Furthermore, this frost correction method naturally causes uncertainty on the obtained value of C. Around 11% of profiles have values of γ between 0.1 and 0.3. In this case, Mariage (2015) estimates that the window frost correction leads to a 30% error on C. A further 3% of profiles have $0.05 \leq \gamma < 0.1$, in which case the error on C can be up to 60%. For $\gamma \geq 0.3$, the C error tends towards the frost-free system constant determination error, which is around 10% (Mariage, 2015). The system constant is used in the calculation of the attenuated scattering ratio, from which all cloud quantities are derived (Sect. 3.2). However, it is difficult to quantify the impact of its error on cloud detection, in part because it depends on the sign of the error. An overestimated C would lead to under-detection of cloud layers, and vice versa. In practice, visual inspection of the profiles indicates that the cloud detection algorithm outlined below is robust to the errors that may be incurred through the window frost correction.

3.1.2 Receiver saturation due to reflective low clouds

The detectors used in the IAOOS lidar are avalanche photodiodes, and can reach saturation. This means that if they are exposed to a signal which is too intense, the photon count goes down. If the saturation is very intense, the photon count can even reach zero (Exc, 2018). Following saturation, the photon number count then slowly increases back up to its normal background value. Saturation is not usually an issue in most lidar operation situations; however during the Arctic summer, background noise levels are high due to shortwave radiation and the reflective sea ice and the signal reflected by the very low cloud cover is often enough to saturate the detector. This problem was observed from the very first deployment of the IAOOS buoys (Mariage, 2015). It translates visually into a lidar signal which dips below background noise levels at a certain altitude, and then slowly increases back to the background. Over the whole IAOOS period, approximately 30% of profiles were concerned by this phenomenon.

A saturated profile may contain some geophysical data above the saturation altitude; therefore, it was important to correct this effect. We hypothesised that the saturated signal S_{sat} resulted from the convolution of the "true" signal S with a saturation impulse response function (IRF):

$$S_{sat}(z) = S(z) * IRF(z)$$

The goal was therefore to deduce S from the measured profile, i.e. S_{sat}. A deconvolution algorithm was therefore put into place (Richardson, 1972; Refaat et al., 2008). The deconvolution process recovered useful signal from the saturated profiles in about a third of cases. In the remaining two-thirds, the "true" signal was only background noise. This represented an appreciable gain in data for the IAOOS campaign.

3.2 Derivation of cloud characteristics from raw lidar data

The lidar profile treatment program is a simplified version of the CALIPSO treatment algorithm described by Winker et al. (2009).

3.2.1 Attenuated scattering ratio calculation

The first step involves calculating the attenuated scattering ratio:

$$SR_{att} = \frac{(S-B)\cdot z^2}{C\cdot O(z)\cdot \beta_m(z) T_m(z)^2} = (1+\frac{\beta_p(z)}{\beta_m(z)})\cdot T_p(z)^2 \quad (1)$$

where

- S is the raw signal;
- B the background noise (calculated as the mean of the raw signal above 20 km, where there is no geophysical signal due to attenuation);
- z the altitude above the lidar, which is at sea level;
- C is the system constant, which varies with the lidar window frost as described above;
- $O(z)$ is the overlap factor between the lidar source and receiver: this factor is determined for each buoy as the average ratio of the raw signal to the calculated Rayleigh signal for very clear, cloudless days. The overlap creates a minimum height underneath which the signal cannot be resolved: a sort of lidar "blind zone";
- $\beta_p(z)$ and $\beta_m(z)$ are the particulate and molecular backscatter ratios at altitude z, respectively;
- T_p and T_m are the particulate and molecular transmission at altitude z, respectively.

The Rayleigh (molecular) backscatter and transmission are calculated according to Bucholtz (1995), using vertical temperature and pressure profiles from ERA5 reanalyses.

3.2.2 Cloud detection

Clouds are then detected by applying a threshold to SR_{att}, since in the absence of particulate attenuation the attenuated scattering ratio will be equal to 1 ($\beta_p = 0$, $T_p^2 = 1$). The initial threshold, S_t, is set to 1.1 at $z = 0$ and increases with altitude in order to take into account that noise increases on the vertical (Winker and Vaughan, 1994).

The base of a feature is detected when seven consecutive points are above the threshold. The top is detected either when SR_{att} has fallen beneath the threshold and has stopped decreasing (a condition inspired by Winker and Vaughan (1994)) or when the signal is below the noise level. The noise level is defined as $2\sigma z^2$, where σ is the standard deviation of the raw signal above 20 km. Assuming gaussian noise, 95% of pure noise fluctuations are therefore beneath this level.

Above the features, SR_{att} will again be constant but equal to $T_f^2(z_{top})$, where z_{top} is the top altitude of the features and T_f its transmission, because of the particle attenuation. This means that new features above this feature will be missed unless the threshold is modified to take the feature attenuation into account. Therefore, above a feature, the threshold is updated to $T_f^2 \cdot S_t$.

Once detected, a feature is determined to be a cloud if its spread, defined as the ratio of maximum feature SR_{att} to average below-feature SR_{att}, is greater than 100 (or 20 for higher-altitude layers for which average below-feature SR_{att} is strongly impacted by noise).

3.2.3 Calculation of optical depth and lidar ratio

When the lidar beam goes through the cloud layer and reaches the particle-free air on the other side, the cloud transmission can be directly calculated as the ratio of the mean SR_{att} above and below the cloud layer over a minimum of 20 points (or 300 m).

However, this was rarely the case during IAOOS, especially in the summer when the noise level is high. Over the whole IAOOS campaign, only 14% of all features were transparent to the lidar. In all other cases, the cloud transmission T_c^2 was calculated from the integrated attenuated backscatter (IAB), assuming a constant lidar - or backscatter-to-extinction - ratio S_c within the cloud layer:

$$IAB = \int_{z_0}^{z_1} \beta_p(z) \cdot e^{-2\int_{z_0}^{z} \eta\alpha_p(z')dz'} dz = \frac{1}{2\eta S_c}(1 - T_c^2) \tag{2}$$

with z_0 and z_1 the bottom and top of the cloud, α_p the particle extinction coefficient and η the multiple scattering coefficient (Platt, 1973). The IAB can then be calculated from the attenuated scattering ratio and molecular backscatter (Winker et al., 2009) :

$$\begin{aligned} IAB \approx & \int_{z_0}^{z_1} SR_{att}(z) \cdot \beta_m(z) dz \\ & - \frac{1}{2}(z_1 - z_0) \cdot (\beta_m(z_0) SR_{att}(z_0) + \beta_m(z_1) SR_{att}(z_1)) \end{aligned} \tag{3}$$

The (relatively few) cases where the cloud layer transmission could be independently calculated were used to derive values of the multiple-scattering lidar ratio $S^* = \eta S_c$ by inverting Eq. (2).

For both Rayleigh- and IAB-derived T_c, the cloud optical depth τ_c can then be deduced:

$$T_c = e^{-\eta \cdot \tau_c} \tag{4}$$

The multiple-scattering coefficient η was assumed constant and equal to 0.8, based on previous analyses of the IAOOS data (Mariage et al., 2017; Di Biagio et al., 2018).

3.2.4 Uncertainty and limits of the method

Equation (2) implies that as $T_c^2 \to 0$, $IAB \to \frac{1}{2\eta S_c}$. This means that for optically thick clouds, a small error on the value of IAB or S_c risks propagating to a large error on COD. The error is also asymmetrical: an overestimation of IAB or S_c yields a much worse result on COD than an underestimation of these same quantities. In practice, if the lidar ratio of a cloud of true optical depth 1.5 is underestimated by 10%, the measured optical depth will be ≈ 1.1. On the other hand, if it is overestimated by the same amount, the measured optical depth will be ≈ 2.2. In some cases, overestimation of lidar ratio or IAB can even lead to negative T_c^2 values, which is non-physical and doesn't allow for the calculation of optical depth. In practice, therefore, this method is appropriate mainly for optically thinner cloud layers. We will refer to "low-IAB" cloud layers, for which the method does not lead to non-physical results (i.e., the cloud layer is thin enough that this method works well). This accounts

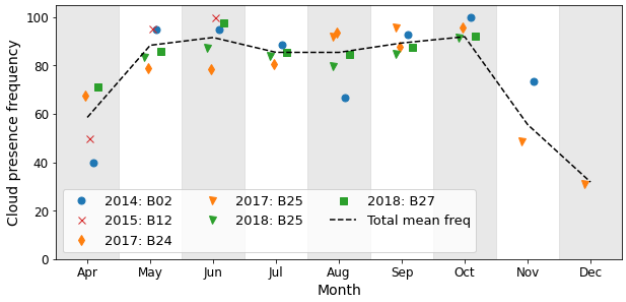

Figure 2. Monthly variation of low cloud frequency, defined as the number of profiles that contain at least one cloud layer with base lower than 2 km divided by the total number of profiles for the month, for five IAOOS buoys. The dashed line represents the total monthly cloud frequency over all IAOOS profiles. It is only calculated for months with more than 30 profiles in total.

for 42% of all features. We will call "high-IAB" cloud layers those for which calculated T_c^2 is negative. These mathematically correspond to clouds with higher IAB, and therefore higher COD, than low-IAB cases. The inclusion of these high-IAB COD values in the statistic will be discussed in Sect. 4.3.

Although uncertain in other respects, this COD calculation method has the advantage of being only faintly impacted by background noise levels. On the other hand, noise levels can have a strong impact on the cloud top determination. Tests with simulated lidar signals indicate that cloud top determination error reaches up to 150 m for typical summer noise levels and optically thicker clouds ($\tau_c \approx 2.5$). This error is much lower for low noise levels, such as are found in the high Arctic during the polar night (October - March). This difference must be kept in mind when interpreting seasonal variation of cloud geometrical thickness (Sect. 4.2).

4 ~~Results & discussion~~Seasonal variability of Arctic low cloud properties during IAOOS

4.1 ~~Seasonal variability of Arctic low clouds and their impact on surface temperatures~~

4.0.1 ~~Frequency of cloud presence~~

4.1 Frequency of cloud presence

IAOOS data confirms that low clouds (i.e., with a base under 2 km) are very frequent in the Arctic, especially in the summer. ~~Global low~~ Average monthly cloud frequency from March to December, defined as the average of monthly ratios of profiles containing at least one cloud with base lower than 2 km to all profiles, is 75%. This value is coherent with previous statistics of cloud fraction above 80°N derived from satellites, for example Wang and Key (2004) and Curry et al. (1996), which usually give a global annual cloud cover of around $60 - 70\%$, with a maximum in summer and a minimum in November - April.

Observed seasonal variation of cloud fraction can differ strongly between satellites (Wang and Key, 2004; Zygmuntowska et al., 2012). Chan and Comiso (2013) found large disagreements between MODIS and CALIOP in the Arctic, for example,

especially over sea-ice and during the polar night. This is because MODIS finds it difficult to differentiate between the surface and the clouds when relying only on IR channels. On the other hand, Blanchard et al. (2014) shows that there is good general agreement and similar trends in cloud fraction over Eureka (Nunavut, Canada) between CALIOP, MODIS, CloudSat and the IIR instrument aboard CALIPSO, with a global maximum in September - November and a minimum in March - May. However, discrepancies between passive and active instruments remain (Blanchard et al., 2014). Ground-based measurements play a key part in quantifying seasonal cloud cover variability in the Arctic, although they are often sensitive primarily to lower-level clouds. Averaging ~~ship and ice-camp data~~ visual observations from ships and ice-camps above 80°N, Hahn et al. (1995) found that cloud cover was globally stable around 60% in winter, increasing to 80% from April to June, and decreasing again from September to November. A maximum of 85% was reached in August/September. The combined lidar-radar measurements at SHEBA give slightly higher values of 70% in winter and 90% in summer, with an earlier transition (February to April) and a peak in September (Intrieri et al., 2002b). ~~The IAOOS~~

The results of IAOOS dataset are shown in Table 3 and Fig. 2. Note here that the number of profiles available for each month is variable, both because of the more favorable operation conditions in the summer and the timing of the buoy deployment (usually in May). As such, there are more than 200 profiles from May to September, around 100 in April and October, and less than 54 in November and December (months with less than 30 profiles, i.e. January, February, and March, are not treated in this article). Care must therefore be taken in analysing the results of late autumn and winter. A 90% confidence interval for the cloud occurrence frequency can be estimated from a Bayesian calculation, assuming that the number of cloudy profiles follows a binomial distribution and supposing an appropriate a priori distribution for the cloud frequency from the literature (Appendix A).

The IAOOS data shows a similar trend as the literature, with generally higher cloud cover values. From May to October, clouds are present over 85% of the time (Fig. 2)~~, decreasing to 60% in April and November, which appear to be the transition months~~. In contrast to the previous ground-based climatologies outlined above, there are two peaks at more than ~~90%~~ 0.9 in the monthly cloud frequency, although they differ little from the summer baseline. The first is in June, ~~although there is strong variability between years and buoys in this month (see below~~which has a mean cloud frequency of 0.92 and a confidence interval of $(0.88 - 0.94)$. The second peak ~~, which is very consistent for every year and buoy, is in October~~is in October, also with a mean cloud frequency of 0.92 but with a slightly wider confidence interval $(0.85 - 0.95)$ because of the lower number of profiles. This is reminiscent of the results of Zygmuntowska et al. (2012), from CALIPSO data, which show a peak in cloud occurrence above ~~90%~~ 0.9 in October. July and August have slightly lower cloud frequency values (0.85 $(0.82 - 0.88)$ and 0.85 $(0.8 - 0.89)$ respectively). However, since there is non negligible overlap between the confidence intervals of June/October and the other summer months, it is difficult to draw solid conclusions as to May - October variability.

~~IAOOS cloud frequency has the greatest interannual variability in spring to early summer (April to June), and appears most consistent in September~~ In the IAOOS dataset, April and November appear to mark a sharp transition in cloud occurrence frequency from the summer values. April has a cloud frequency of 0.59 $(0.52 - 0.67)$ while the cloud frequency in November is 0.56 $(0.48 - 0.68)$. While the confidence intervals are quite wide here due to the lower number of profiles, there is no overlap with the summer confidence intervals. This suggests that the lower cloud frequencies observed during the months of April and

November is meaningfully different from that of the months of May through October. December cloud frequency is lower still, at 0.32 (0.29 – 0.51). Note however the width of the confidence interval and the fact that the December data corresponds to a single year of measurement (2017).

It is not possible to robustly quantify interannual variability in Arctic cloud cover from the IAOOS dataset since there are at most four years of data for each month. Qualitatively, however, the April - ~~October~~May transition in cloud frequency observed by the buoys is quite variable. In 2014, the B02 buoy observed a very sharp spring transition in cloud frequency: from ~~40% in April~~ 0.4 (0.35 – 0.6) in April 2014 to more than ~~90%~~ 0.9 (0.89 – 0.97) in May and June 2014 (blue circles, Fig. 2). On the other hand, this transition was much more gradual in 2017 (buoy B24, orange diamonds~~: the June~~). The June 2017 cloud frequency is less than ~~80%)~~0.8 (0.69 – 0.85), overlapping significantly with the May 2017 cloud frequency confidence interval of (0.56 – 0.78). This is not an effect of spatial variability as both B02 and B24 were drifting in the Atlantic sector of the Arctic (Fig. 1).

It has been observed from satellite data that the Atlantic sector is the cloudiest part of the Arctic Ocean (Liu et al., 2012; Wang and Key, 2004). This is linked to the low pressure systems and the storm tracks arriving from the northern Atlantic Ocean. ~~This is not supported by the IAOOS data: there is little difference in cloud frequency between buoy B25, which drifted to the Laptev sea from summer to autumn 2018, and buoy B27, which at that time was drifting in the Atlantic sector. However~~Since most of the IAOOS buoys drifted in this sector, the IAOOS dataset ~~lacks spatial coverage for a robust determination of~~ must be regarded as most representative of these specific conditions, and not of the ocean-wide ~~variability of cloud cover~~cloud characteristics.

~~The~~ Furthermore, the results above pertain to the low cloud cover, i.e. clouds with a base underneath 2 km. Clouds with a base between $2 - 5$ km are much rarer in the IAOOS dataset, occurring only 3% of the time from March to December, with a peak at 8% in July. However, as the lidar signal is often dampened by the first cloud layers, IAOOS statistics of cloud cover above 2 km are expected to be biased low.

4.1.1 ~~Cloud geometrical properties~~

4.2 Cloud geometrical properties

Multi-layer clouds were detected 7% of the time by the IAOOS lidar over the course of the campaign. This value is small compared to previous observations: for example, Liu et al. (2012) find that multi-layer clouds are present 20% of the time year-round, with very low seasonal variation. These results are drawn from satellite observations and Liu et al. (2012) note that they are also underestimated. Ground-based measurements generally attest to frequent multilayering in the summertime, with layers separated by several hundred meters (Curry et al., 1988, 1996). SHEBA measurements even show that multi-layer clouds exceeded single-layer clouds in June and July 1998, and occurred on average 45% of the time over the whole experiment period (Intrieri et al., 2002b). IAOOS measurements also attest to a higher frequency of multiple layered clouds in summer: they occur more than 10% of the time July - October, and only 4% of the time in April and May (Table 2). ~~November, December and March multilayered cloud occurrence is non-significant~~Only one IAOOS profile contains multilayered clouds in November,

Month	N_p (#)	$\frac{N_{ml}}{N_{profiles}}$ (%)	First cloud base (%)			
			$<$ 120m	120− 500m	500m −2km	2− 5km
~~Mar 28 0 57 29 7 7~~	94	4	96	0	2	2
Apr						
May	359	4	95	2	1	1
Jun	330	8	87	8	3	1
Jul	342	14	93	1	3	3
Aug	205	12	91	2	5	2
Sep	251	10	90	5	4	1
Oct	98	13	98	2	0	0
Nov	54	2	93	3	3	0
Dec	44	0	93	7	0	0

Table 2. Cloud multiple layer and base characteristics for all profiles from ~~March~~ April to December. N_p is the total number of lidar profiles for each month (for all years and buoys), and N_{ml} is the number of profiles containing multilayered clouds. The last four columns represent the % of first layer cloud bases in each altitude range. The 120 m cutoff corresponds to the minimum altitude at which the lidar overlap factor can be corrected for all buoys. Cloud bases above 5 km, which correspond to "high-level" clouds in many reanalyses such as ERA5, are not included because the lidar range in perfectly clear daytime conditions is only 4.4 km (Sect. 2.1).

and none in December. Despite the low number of total profiles in these months, these values are different from the July multilayered cloud frequency at a statistically significant level: for November, Fisher's exact test yields a p-value of 0.007 (Fisher, 1922). IAOOS measurements strongly underestimate frequency of multilayered clouds due to the fact that the lowest cloud layer entirely attenuates the lidar signal in most profiles. Furthermore, cloud layers separated by less than 300 m were counted as one in the IAOOS data treatment in order to have a better estimation of cloud transmission (Sect. 3.2.3). However, the robust measurement of the geometry of the first cloud layer derived from IAOOS measurements base is a useful statistic. Indeed, the base of the lowest cloud layer is expected to have the strongest impact on surface radiative fluxes as compared to higher cloud layers. Hereafter, all cloud statistics refer to single cloud layers; in most cases, the lowest.

~~It is clear from the IAOOS database that Arctic clouds~~ Clouds in the IAOOS dataset are extremely low, with little seasonal variability. From April to December, at least 85% of first layer clouds have a base below 120 m, which is the minimum altitude at which the lidar overlap factor can be corrected for all buoys (Table 2). The median base altitude is therefore at 120 m in nearly every month. ~~In March, only 57% of cloud bases are below 120 m. Another 29% of first layer cloud bases are between~~

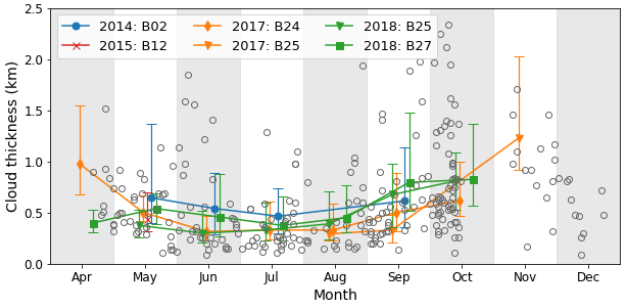

Figure 3. Monthly evolution of first layer cloud geometrical thickness (in km), for five IAOOS buoys. The markers represent the median value, and the whiskers indicate the 25th and 75th percentiles. The open circles represent individual cloud thickness values where the lidar signal sees through the cloud layer, i.e. the cloud top is clearly detected. The median, 25th and 75th percentiles are only calculated when more than 15 data points are available.

~~120 and 500 m, which still corresponds to low level, likely boundary layer clouds (note however the low number of profiles in this month). This is in line with the results of previous measurements campaigns.~~ During ASCOS, which took place in August 2008, the lowest cloud base distribution peaked beneath 100 m (Tjernstrom et al., 2012). Median first cloud base from SHEBA measurements (Shupe et al., 2007) was also less than 120 m for all months except March (179 m) and April (209 m). Nevertheless, higher-altitude first cloud layers were more frequent than during IAOOS, especially in spring to early summer (Intrieri et al., 2002b).

On the other hand, Fig. 3 highlights a significant difference in measurements of single-layer cloud geometrical thickness between summer (May to September) and the ~~shoulder months (~~months of April, October ~~/November)~~and November. The median cloud thickness from June to August ranges between 360 and 390 m, whereas it is nearly 750 m in October and March, and more than 1 km in November. This difference appears significant at a statistical level. The Mann-Whitney U for the July and October cloud thickness distributions was 9834.5 (with sample sizes $n_1 = 355$ and $n_2 = 104$), yielding a p-value < 0.001 (Mann and Whitney, 1947). The same is true for July and April ($U = 5940.5$, $n_1 = 355$ and $n_2 = 60$, p-value < 0.001).

As explained in Sect. 3.2.3, it is expected that summer cloud thickness would be underestimated by up to 150 m due to higher noise levels in this period. However, this is too small an error to explain the different median values observed between summer and spring/autumn. Furthermore, these values and trends are coherent with previous studies of single-layer clouds at Barrow and Eureka. For example, the average thickness of single-layer clouds at Barrow from June to August 2000 was 320 m while the September average was 550 m (Dong and Mace, 2003). Over the 2005 to 2008 period the average single-layer mixed-phase cloud thickness at Eureka varied from 200 m to 700 m with maxima in autumn and minima in spring (de Boer et al., 2009). Total thickness of all clouds, single-layered or not, may however be much larger. During SHEBA, median total cloud thickness from radar data was above 1 km in every month, with peaks at around 3 km in April and October (Shupe et al., 2007). These values are from 3 (March/April) to 7 (July/August) times larger than the IAOOS monthly median values.

4.2.1 ~~Cloud optical properties~~

4.3 Cloud optical properties

As noted in Sect. 3.2.3, cloud layers for which both IAB and T_c^2 are determined independently can be used to calculate the multiple-scattering lidar ratio S^*. In total, there were ~~222~~ 207 such cloud layers during the IAOOS period, covering the March to December period. They are shown in Fig. 4a, along with the median and the 25th and 75th percentiles for each month. The global median is 17.5 sr, with 90% of values falling in the $7-38$ sr range. Although the spread is quite large, these results are consistent with cloud lidar ratio values found in the literature. For example O'Connor et al. (2004) found that S^* values ranged between 14.5 and 16.5 sr for low water clouds; for ice or mixed-phase clouds, the range was $5-40$ sr, very similar to IAOOS results.

The seasonal variation of S^* is statistically significant: the median S^* for the summer months (JJA) was 23 sr versus 15.5 sr in the autumn (SON). The Mann-Whitney U is 4953.5, with $n_1 = 67$, $n_2 = 98$, yielding a p-value of ~~$< 10^{-5}$~~ < 0.001 (Mann and Whitney, 1947). There are two possible causes for the observed variability in $S^* = \eta S_c$: changes in the multiple scattering coefficient η or S_c. η decreases with cloud temperature (Garnier et al., 2015) while S_c depends on cloud microphysical properties, among which cloud droplet effective radius and phase. In the absence of additional measurements, it is difficult to determine which one has the largest impact here, as well as the ultimate physical cause of variation. ~~For example, the very high values observed in March might be due to the higher occurrence of ice particles in clouds during this period, but could also be suggestive of Arctic haze. Indeed, Lubin and Vogelmann (2006) found evidence that the cloud droplet effective radius is lower, and S_c is therefore higher, when aerosol condensation nuclei concentrations are high in the Arctic, independent of other seasonal or temperature effect. In any case, the~~ The monthly median values were then used to calculate COD (Sect. 3.2.3).

The average single-layer COD during IAOOS excluding high-IAB cases was 0.9, with values ranging from 0.3 to 2.1. These values are small when compared to previous satellite and ground based studies in the Arctic. But as noted in Sect. 3.2.4, the retrieval method used for calculating COD from the IAOOS lidar data when the signal is fully attenuated is not suited to optically thick clouds: the rough upper bound of COD which can be measured through this method is 2. As almost 20% of cloud layers observed during the campaign were high-IAB, this likely has a non-negligible impact on results. Furthermore, contrarily to satellite data, IAOOS values are single-layer, not whole column, COD. The contribution of the first layer to total column COD is discussed in Sect. 5.3. It is therefore understandable that previous studies gave larger COD values. For example, Curry et al. (1996) cites a range of $2-24$ with an average of 8 in summer. Wang and Key (2004) also finds that monthly mean COD (from 1982 - 1999) varied from 4 to 6 in the AVHRR data over the Arctic Ocean. From ground-based lidar measurements at SHEBA, Turner (2005) shows that 63% of clouds were single-layer with an optical depth < 6, and that optically thin clouds tended to be predominantly composed of ice.

Single-layer COD appears to vary seasonally (Fig. 4b). Excluding high-IAB cases, the monthly median COD appears to be almost constant from April to September, and largest in October - November (filled circles). However, this is in part because of the low noise levels in these months as compared to the summer. In ~~March and~~ October - December, i.e. the months with no sunlight, more than 50% of cloud layers were transparent to the lidar. This proportion is less than 10% in May to July.

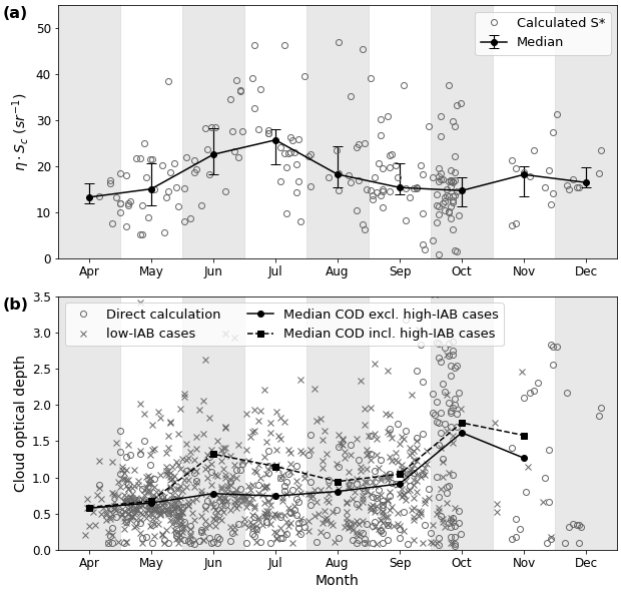

Figure 4. Panel a: monthly variations of lidar ratio values over the IAOOS campaigns. The open circles represent the measurements. The filled markers represent the monthly medians, with the whiskers indicating the 25th and 75th percentiles. Panel b: monthly evolution of single-layer COD, for five IAOOS buoys. Open circles represent the Rayleigh-derived cloud optical depths. Crosses correspond to the low-IAB COD values (Sect. 3.2.4) Filled markers represent the monthly medians, when high-IAB cases are excluded (circles) or included (squares). These medians are calculated when more than 15 data points are available.

The COD can therefore be directly calculated for optically thick clouds from late September - ~~March~~ December but not in other months. This is visible in Fig. 4b: in late September/October, there is a sudden apparition of directly-calculated COD values (open circles) greater than 2. The IAB method, which is an alternative to the direct method of calculating COD when the signal is fully attenuated by the cloud, is mainly suited to optically thin clouds (Fig. 4, grey crosses). This creates bias between summer months, for which the COD calculation is limited by noise levels to optically thin clouds, and October - December, during which higher COD values can be calculated.

To overcome this problem, the COD of high-IAB cloud layers was set to 2. This value was chosen as it is the 95th percentile of CODs calculated for low-IAB layers, and high-IAB cloud layers are ~~globally~~ as a group expected to have higher COD than low-IAB ~~layerS~~layers. The monthly median COD was then calculated including these high-IAB cases (Fig. 4, filled squares). This correction is not quantitatively robust as the value of 2 is arbitrarily chosen, not calculated. However, it accounts for the fact that high-IAB cloud layers exist, and are expected to have higher COD than low-IAB cloud layers, in the calculation of the median. This is helpful for examining the seasonal trend~~.~~, which otherwise is biased by the presence of noise.

It creates a significant difference in June and July, the months in which the percentage of high-IAB cloud layers is the highest. With this correction, the median monthly COD exhibits two peaks (June and October) and a minima in April. The October peak is however still the annual maximum~~.~~

Month	Number of profiles	Cloud fraction (%)	Median temperature (°C)		
			Cloudy	Cloudless	Δ
~~Mar 28 46 -23.2 -29.9 6.8~~ Apr	94	59	-17.7	-21.2	3.5
May	359	88	-9.9	-13.6	3.7
Jun	330	92	-1.5	-1.5	0
Jul	342	85	-0.1	-0.5	0.4
Aug	205	85	-0.9	-1.1	0.2
Sep	251	89	- 3.7	-6	2.3
Oct	98	92	-6.6	-14.6	8.
Nov	54	56	-16.7	-25	8.4
Dec	44	32	-27.9	-28.5	0.6

Table 3. Monthly median temperature for cloudy and cloudless profiles from ~~March~~ April to December over the whole IAOOS period. Cloudy profiles contain at least one cloud with a base underneath 2 km. Cloudless profiles contain no clouds, or (very rarely) higher level clouds. Δ is the difference between cloudy and cloudless profile median temperatures.

, and does not appear to be strongly impacted by the inclusion of high-IAB cloud layers. Previous satellite measurements have exhibited a pattern of higher COD in ~~the shoulder seasons~~spring and autumn, for instance May and October for the AVHRR data (Wang and Key, 2004) over the Arctic Ocean. ~~IAOOS measurements confirm that there is a~~ The IAOOS dataset exhibits this October peak in single-layer COD~~in October, and possibly in June~~. Another peak in June appears possible, although the IAOOS measurements are very uncertain in this month.

4.3.1 ~~Impact of clouds on surface temperatures~~

5 Cloud impact on surface temperatures and radiative balance

5.1 Impact of clouds on surface temperatures during IAOOS

IAOOS lidar profiles can be split into two groups: ~~those that contain a~~ "cloudy" profiles containing at least one low cloud with a base < 2 km and ~~those that don't.~~ "cloudless" profiles which contain either no cloud, or higher level clouds. Note that less than

2% of all clouds had a base higher than 2 km (Sect. 4.2). The temperatures measured by the buoy meteorological station during each lidar profile acquisition can be compared to estimate the effect of the presence of low clouds on surface temperatures.

The 2 m temperature distributions of cloudy and cloudless profiles differ significantly in October-November and ~~March-April~~ April (Table 3). The Mann-Whitney test p-value is less than 0.05 (~~$< 10^{-4}$~~ < 0.001 for November) and the common language effect size is more than 70% (> 80% for October and November). For all of these these months, the 2 m temperature is much lower for cloudless than for cloudy profiles. Indeed, the difference between the medians is of 8°C for the autumn months and around $4 - 7$°C in the spring (Table 3). This difference is probably not due solely to radiative processes, as cloudy situations in the Arctic winter are also associated with the passage of storms, which bring warm, moist air with them. However, as seen in Sect. 4.3, IAOOS-measured CODs are larger in October/November than April. Since emissivity increases with optical depth, this supports a larger surface warming in autumn than in spring.

The months with the lowest median temperature difference between cloudy and cloudless profiles are June, July and August. In fact, the temperature distributions are statistically indistinguishable in these months from the relatively few measurements we have access to here. In particular, there is no month in which cloudless profiles are warmer than cloudy profiles, even though clouds are known to exert negative radiative forcing from late June to early July. ~~The reasons for this are explored in Sect. 5.3 by investigating the summer radiative balance.~~

As noted before, clouds are naturally not the only factor impacting surface temperatures or even the downwards longwave radiative flux. Large-scale circulation is also important: for example, high geopotential at 200 hPa is linked to a warming of the troposphere through subsidence, which increases the longwave radiative flux received at the surface (Ding et al., 2017). It is therefore important to check that cloudy and cloudless lidar profiles do not sample different surface pressures. The IAOOS buoys were equipped with barometers as well as temperature sensors. It appears that surface pressures for cloudy and cloudless profiles are not different at a statistically significant level, with the exception of August and November. In both of these months, the lidar profiles that contain clouds appear to coincide with markedly higher surface pressures than those that don't contain clouds (+12 hPa, Mann-Whitney test p-values < 0.005). As surface temperatures in the two groups differ strongly in November but not in August, however, surface pressure does not appear to be a confounding factor for surface temperature and cloud occurrence.

In the following sections, we look at the summer surface radiative balance in order to gain a better understanding of the mechanisms behind this seasonal variation in temperature difference between cloudy and cloudless profiles. First, the link between the net surface longwave flux and the presence of clouds is investigated (Sect. 5.2.1) from compared N-ICE and IAOOS measurements. Then, the influence of other factors such as solar zenith angle, temperature and COD on downwards shortwave and longwave fluxes during the N-ICE2015 April to June period is explored (Sect. 5.3). Lastly, the discussion of the net cloud radiative forcing at the surface is extended to the months of July and August using a simple parametrisation (Sect. 5.4).

5.2 ~~Radiative modes in~~ Influence of the ~~Arctic~~presence of clouds on the surface net longwave radiative flux

5.2.1 Identification of two summer longwave radiative modes from IAOOS and N-ICE data

The 2 m temperature difference between cloudy and cloudless autumn/winter profiles exposed in Sect. 5.1 is consistent with previous studies. Indeed, it is now well attested that the Arctic climate exhibits two distinct states during the winter, which are distinguished through the surface net longwave flux (netLW) values. The bimodality of netLW was first observed during the SHEBA measurement campaign over the January-February 1998 period (Stramler et al., 2011) and has since been confirmed Arctic-wide by satellite observations (Cesana et al., 2012). The "radiatively clear" mode (netLW < -30 W m^{-2}) is associated with strong radiative cooling, high pressures and low temperatures. Clouds may be present but are optically thin and mainly composed of ice. The "opaquely cloudy" mode is characterised by low pressures and relatively higher temperatures, and often associated with so-called "moisture and temperature intrusions" from the midlatitudes (Woods et al., 2013). Clouds are then liquid or mixed-phase, and optically thick. These intrusions are one of the main drivers of interannual variability of netLW, with a contribution of about 40% (Woods et al., 2013).

Here, we used radiative flux data from the N-ICE field campaign (second period, April - June 2015) to complement the IAOOS lidar observations (Hudson et al., 2016). Measurements from the first period (January to March 2015) of N-ICE have already been shown to confirm the wintertime bimodality of the netLW distribution (Graham et al., 2017). This result is replicated in Fig. 5b. A more striking point is that the netLW distribution is also bimodal in spring to early summer (Fig. 5c). During this period, netLW values range from -90 to 0 W m^{-2}. The most predominant netLW mode, containing around 80% of data points, is centered around -11 W m^{-2}, while the other is centered around -72 W m^{-2}. As a IAOOS buoy drifted near the main ice camp during April-June 2015, the IAOOS profiles were used to determine whether the sky was cloudless or cloudy at a given moment. The comparison with netLW measurements is represented in Fig. 5a. Low netLW values (< -60 W m^{-2}) are associated with IAOOS profiles that are cloudless at least up to ≈ 5 km, which is the maximum range of the lidar. Meanwhile, profiles containing at least one low level cloud (grey lines) corresponded to netLW values larger than -20 W m^{-2}.

This shows that the observed low netLW mode corresponds to a cloudless state and the high netLW mode to a cloudy state. By analogy with the previously established winter radiative states, we name the spring/summer low-netLW mode "radiatively clear" and the high-netLW mode "opaquely cloudy". However, these two modes differ from their winter analogues in several ways. Firstly, the netLW mode values are lower than in the winter~~, due to the higher surface temperatures in spring/summer. Secondly, the difference between the two states is ≈ 60 W m^{-2}, much larger than in the winter. This implies that clouds have a larger longwave warming effect in the spring/summerthan in the winter, probably linked to larger liquid contents and higher cloud temperatures in this season. Thirdly~~. Indeed, both the downwards and upwards components of the longwave flux (LWd and LWu) increase from winter to summer. However, LWu increases more than LWd in both modes, causing a shift to lower netLW values. Secondly, the opaquely cloudy mode is much more frequent in spring/summer than in the winter, representing a large majority of cases. This is coherent with the fact that cloud frequency is much higher in spring/summer than in winter, with a transition in April (Sect. 4.1). Thirdly, the difference between the two states is ≈ 60 W m^{-2}, much larger than in the winter.

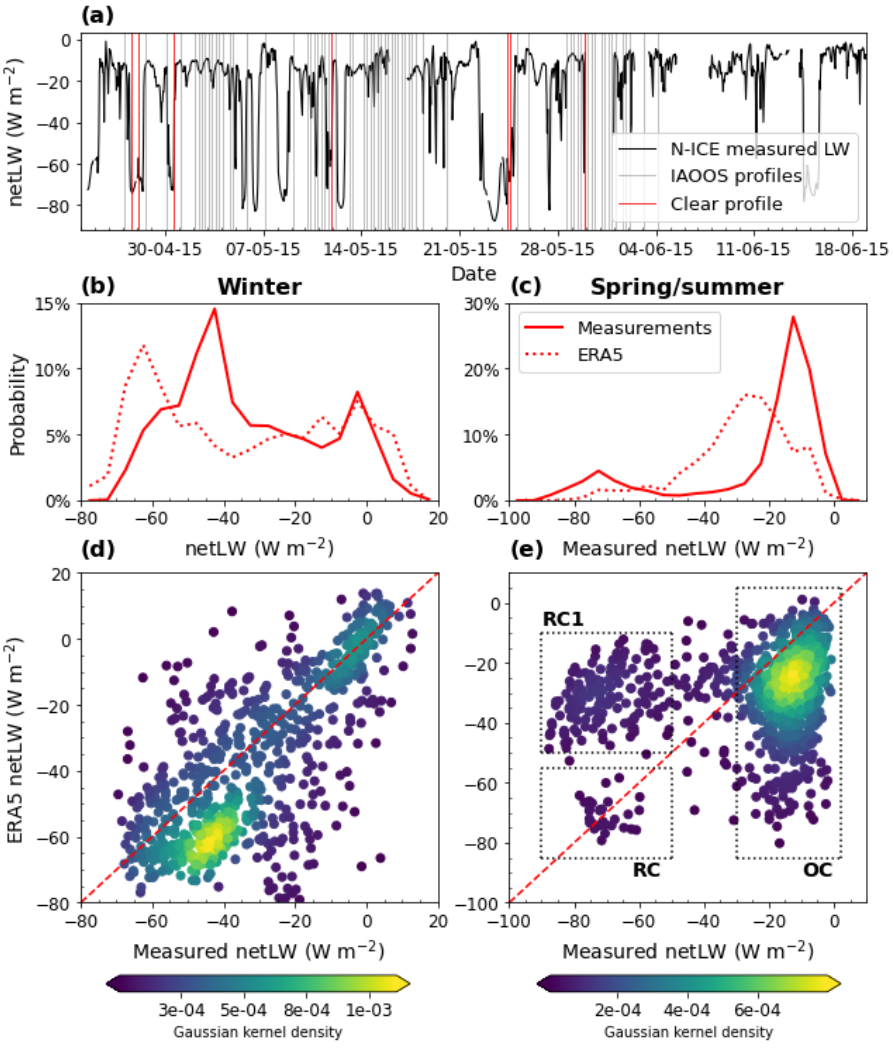

Figure 5. Panel a: time series of surface net longwave measurements during the N-ICE field experiment (second period, April-June 2015). ~~IAOOS buoys were deployed near the main ice camp where radiative fluxes were measured.~~ The vertical lines indicate the time of IAOOS lidar profiles, with red lines corresponding to cloudless profiles. Panels b and c: histogram of the measured (filled line) and ERA5 (dashed line) net longwave flux during the N-ICE winter (b) and spring/summer (c) campaign periods. Panels d and e: hourly ERA5 vs measured net longwave in during the N-ICE winter (d) and spring/summer (e) campaign periods, with red dashed line indicating the 1:1 line. The colour corresponds to point density as calculated by a Gaussian kernel. For panel (e), three zones have been outlined. Zone "OC" contains points belonging to the opaquely cloudy mode of the measured netLW distribution. Zones "RC1" and "RC2" contain points belonging the radiatively clear mode of the distribution in April and May (RC1) and June (RC2).

This implies that clouds have a larger longwave warming effect in the spring/summer than in the winter, probably linked to larger liquid contents and higher cloud temperatures in this season.

5.2.2 ~~Comparison~~ Representation of the two modes in the ERA5 ~~to N-ICE measurements~~reanalyses

The two atmospheric winter states (radiatively clear and opaquely cloudy) are not well reproduced by models (Cesana et al., 2012; Pithan and Mauritsen, 2014; Graham et al., 2017). In fact, it has been suggested that representing the bimodality of the netLW, pressure and temperature distributions in the wintertime is a key quality criterion for models. ERA-Interim and its successor, ERA5, are among those that partially achieve this (Graham et al., 2017). This is visible in Fig. 5d. The opaquely cloudy state lies on the 1:1 line and is therefore well represented. However, the radiatively clear netLW values are underestimated by about 15 W m^{-2}. This is mainly due to an error in the upwards component of the longwave flux. Indeed, ERA5 overestimates the clear mode 2 m temperature by about 5 K; its measured value is $T_{meas} = -32$°C (Graham et al., 2017), while the ERA5 clear mode temperature is $T_{ERA5} = -27$°C. This leads to an error on the longwave upwards flux at the surface (LWu) of:

$$\begin{aligned}\Delta(\mathrm{LWu}) &= 4\epsilon\sigma \cdot (T_{ERA5} - T_{meas}) \cdot (T_{meas} + 273.15)^3 \\ &\approx 15.6 \text{ W m}^{-2}\end{aligned} \tag{5}$$

with ϵ the surface emissivity, which is assumed to be 0.99 (Walden et al., 2017). The result of Eq. (5) is in line with the observed netLW error. It should be noted that this overestimation of near-surface temperatures in clear, stable winter conditions, leading to an underestimation of netLW, is a feature shared by the six reanalyses evaluated by Graham et al. (2019) using the N-ICE campaign data.

In the spring/summer period, Graham et al. (2019) further notes that ERA5 is the least biased of the six evaluated reanalyses with regards to netLW, but has the worst correlation coefficient ($R = 0.15$). Indeed, we find that ERA5 fails to represent the two spring/summer netLW modes. The ERA5 netLW distribution is not bimodal (Fig. 5c) and does not align with the measurements (Fig. 5e). Three zones have been outlined on figure 5e to aid with the following discussion of ERA5 spring/summer netLW error. Zone OC corresponds to measured opaquely cloudy values over all spring/summer. The opaquely cloudy mode is somewhat reproduced by ERA5 (yellow dots denoting a peak in the calculated gaussian kernel density), although its values are underestimated by 11 W m^{-2} on average. The two other boxes correspond to measured radiatively clear values from April/-May (RC1) and June (RC2) respectively. June values are well reproduced by ERA5. However, ERA5 vastly overestimates radiatively clear netLW in April and May: there is a 40 W m^{-2} difference with measurements in these month (Fig. 5e, RC1).

The difference in ERA5 netLW values between radiatively clear April/May (RC1) and June (RC2) points is due to the downwards component of the longwave flux (LWd). ERA5 LWd is fairly close to measured values in RC2, but is overestimated by ≈ 53 W m^{-2} in RC1. This is partly compensated by a 14 W m^{-2} error on LWu in April/May, similar to what is observed during the winter. Ultimately, the overestimation of LWd in RC1 is due to a faulty representation of cloud fraction in April/May. The ERA5 mean low cloud cover in RC1 is 0.96, even though measurements indicate a radiatively clear, and therefore cloudless, situation. On the other hand, mean low cloud cover in RC2 is 0.06: ERA5 has correctly identified that the sky was cloudless.

~~The logical conclusion is that~~ In conclusion ERA5 ~~overestimates~~ overestimated low cloud cover in April and May, but not June, leading to the observed errors in netLW. ~~This may ultimately be due to an error in the satellite data that is assimilated by the ERA5 reanalyses. Indeed, as noted in Sect. 4.3, cloud fraction and optical depth is often overestimated by satellite~~

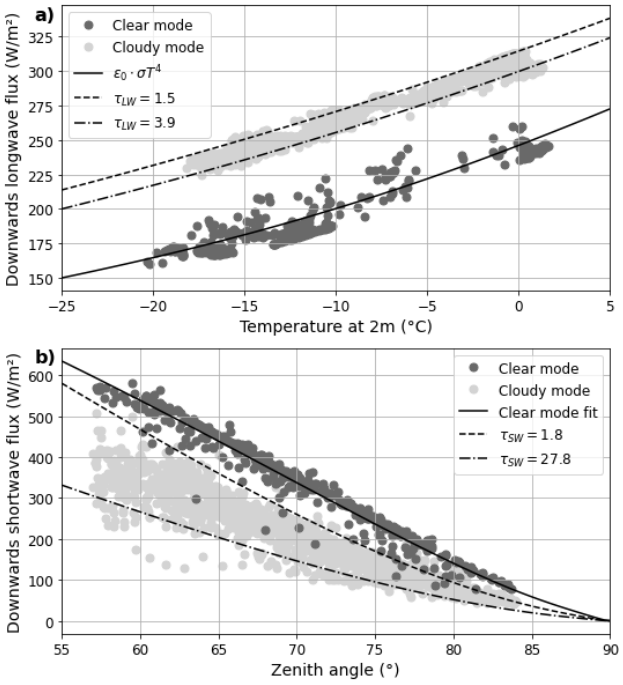

Figure 6. Panel a: ~~evolution~~ longwave downwards radiative flux with near-surface (2 m) temperature as measured during the spring/summer period of the N-ICE field campaign. Dark grey points correspond to values for which $\mathrm{netLW} < -50$ W m^{-2} ("radiatively clear" mode) while for light grey points $\mathrm{netLW} > -20$ W m^{-2} ("opaquely cloudy" mode). The filled line correspond to the results of a simple parametrisation of LWd (Eq. (6)) in the absence of clouds, while the dashed lines represent the results of the parametrisation for $\tau_{LW} = 1.5$ and $\tau_{LW} = 4.1$. Panel b: same, for shortwave downwards radiative flux vs solar zenith angle. The dashed lines are the results of Eq. (7) for $\tau_{SW} = 1.7$ and $\tau_{SW} = 28.2$. For both panels, points are 30-minute averages of measurements.

~~measurements at high solar zenith angles over bright surfaces (Chan and Comiso, 2013). These are the predominant conditions in April and May, whereas in June the solar zenith angle is lower and areas of open water start to appear, decreasing the surface albedo~~More investigation is required as to the ultimate source of this error.

5.3 ~~Cloud impact~~ Variability of cloud impacts on the ~~summer surface~~ downwards radiative ~~budget~~fluxes during N-ICE2015

~~Section 5.2.1 showed that the spring/summernetLW distribution exhibits two modes, termed radiatively clear ($\mathrm{netLW} < -50$ W m^{-2}) and opaquely cloudy ($\mathrm{netLW} > -20$ W m^{-2}). These were linked respectively to the absence and~~ In the Arctic summer, clouds impact the surface radiative budget in two competing ways: they have a longwave warming effect and a shortwave cooling effect. In Sect. 5.2.1, the N-ICE2015 April-June netLW distribution was shown to be bimodal, with the first mode corresponding to the presence of clouds in the ~~lidar profiles~~ IAOOS profiles and the second to their absence. However,

~~Sect. 5.1 showed that there is very little difference between 2 m temperatures of cloudless and cloudy profiles in the summer. A more complete analysis of the summer surface radiative budget is therefore required.~~

~~In the Arctic summer, clouds impact the~~ other factors than the absence or presence of clouds may impact the surface ~~radiative budget in two competing ways: they have a longwave warming effect and a shortwavecooling effect.~~ radiative fluxes, both shortwave and longwave. In this section, the influence of variables such as the solar zenith angle, COD and surface temperature on the downwards fluxes (both longwave and shortwave) from the N-ICE2015 April-June period is explored and parametrisations of these fluxes are introduced.

The longwave effect depends on cloud temperature and phase. Warm, liquid-containing clouds are optically thicker and have much more radiative impact than cold, ice-containing clouds (Shupe and Intrieri, 2003). This is most likely the reason behind the greater difference between netLW modes observed in the spring/summer (≈ 60 W m^{-2}) N-ICE measurement period as compared to the winter (≈ 40 W m^{-2}). The shortwave radiative forcing ~~also~~ depends on cloud characteristics as optically thick clouds have higher albedos. It also depends on the solar zenith angle θ and, to a lesser extent, the surface albedo α, due to reflections between the bright surface and the clouds (Shupe and Intrieri, 2003).

As shown in Sect. 5.2.1, netLW values can be used to discriminate between "radiatively clear" and "opaquely cloudy" instants. The downwards longwave (LWd) and shortwave (SWd) flux components in ~~the radiatively clear and opaquely cloudy modes can be~~ these two modes are then compared in order to evaluate the impact of clouds on the surface. We will use the following simple estimates of LWd and SWd as a complement to the N-ICE flux measurements (Hudson et al., 2016).

– Schematically, the atmosphere can be seen as a cloud layer with emissivity ϵ_c overlying a cloudless atmospheric layer with emissivity ϵ_0. If both layers are emitting at temperature T_{2m}, this yields the following expression for LWd:

$$\mathrm{LWd} = [\epsilon_0 + \epsilon_c(1-\epsilon_0)] \cdot \sigma \cdot T_{2m}^4 \tag{6}$$

The cloud emissivity can simply be expressed as $\epsilon_c = 1 - e^{-\tau_{LW}}$ with τ_{LW} the longwave COD. Several simple parametrisations exist for ϵ_0; here, we choose $\epsilon_0 = 0.83 - 0.18 \cdot 10^{-0.067 e_0}$, with e_0 the near surface water vapour pressure, which was fitted from summer data at Sodankylä, Finland (Niemelä et al., 2001a). This shows good correspondence to the N-ICE clear mode data (Fig. 6a). In fact, equation (6) corresponds to a model introduced by Schmetz et al. (1986) under two simplifying assumptions. First, that the cloud cover is equal to 1, which is reasonable in the cloudy mode. Second, that the cloud base and two-meter temperatures are approximately equal. This is justified by cross-comparison of the N-ICE (second period) radiosonde data with the IAOOS lidar profiles: the overwhelming majority of lowest layer clouds have a base beneath 120 m and the median difference between surface and 100 m temperature in the radiosonde profiles is only 1.3°C (with 90% of values falling in the range $0.6 - 2$°C).

– SWd can be calculated from the downwards shortwave flux in the absence of clouds F_0 and the cloud correction or cloud broadband transmittance factor T_c:

$$\mathrm{SWd} = \mathrm{F}_0(\theta) \cdot T_c(\theta, \tau_{SW}, \alpha) \tag{7}$$

F_0 depends on atmospheric gas and aerosol content and is usually parametrised to fit to local data (Reno et al., 2012; Kambezidis et al., 2017). Here, the fit to N-ICE clear mode data is shown on Fig. 6b (filled black line). T_c has been modeled in numerous ways, the simplest depending solely on cloud cover (Niemelä et al., 2001b), while more complicated expressions have been derived from the output of radiative transfer models. Here we used the parametrisation of Fitzpatrick (Fitzpatrick et al., 2003), which assumes a cloud cover of 1 and depends on the solar zenith angle θ, the surface albedo α and the shortwave COD τ_{SW}. We chose to use a fixed value of $\alpha = 0.8$, as the measured albedo over the N-ICE second period varied from $0.75 - 0.84$ and the model performs poorly for albedos above 0.83 (Fitzpatrick et al., 2003).

Downwards longwave radiative flux increased with near-surface temperature T_{2m} and downwards shortwave flux decreased with θ in both radiatively clear and opaquely cloudy modes during the N-ICE April-June measurement period (Fig. 6). This evolution is well reproduced by Eqs. 6 and 7. Furthermore, there is a marked difference in downwards flux between points identified as radiatively clear and opaquely cloudy for both the longwave and shortwave components. In accordance with a cloud longwave warming effect, radiatively clear LWd values are uniformly lower than the opaquely cloudy values for each T_{2m} (Fig. 6a). As netLW is the quantity used to discriminate between clear and cloudy points, this is expected. On the other hand, radiatively clear SWd values are higher than opaquely cloudy SWd values for each θ (Fig. 6b). This corresponds to the shortwave albedo effect, i.e. clouds reflect solar radiation back to space. The magnitude of this shortwave ~~cooling~~ cloud albedo effect is variable, even for a fixed solar zenith angle. As a first order approximation, this variation is due to the cloud optical properties as the albedo varied little over the measurement period. Equation (7) reproduces the spread of observed values for τ_{SW} between 1.7 to 28.2, a range which is coherent with total column COD values from previous studies (Sect. 4.3). In contrast, the longwave warming effect (i.e., the difference between the dashed/dotted and solid lines in Fig. 6a) varies little either as a factor of T_{2m} or τ_{LW}, and remains close to 60 W m^{-2}.

COD variations therefore have a non-negligible impact on the surface radiative balance. For $\theta = 60°$, for example, there is an approximately 200 W m^{-2} difference in SWd between the optically thinnest and thickest clouds. This translates into a total shortwave cloud forcing that ranges between -20 to -60 W m^{-2}, assuming an albedo of 0.8 (typical of the N-ICE campaign April-June period). This range is significant when it is contrasted to the typical longwave forcing of ≈ 60 W m^{-2}: even for $\theta = 60°$, only ~~optically thick clouds can have a net radiative cooling effect over high-albedo sea ice. Thinner clouds will continue~~ the optically thickest clouds could contribute to cool the surface during the April-June N-ICE2015 campaign period. Most clouds continued to warm the surface. This ~~explains that averaged over the IAOOS campaign, the 2 m temperature of cloudless profiles is not different at statistically significant level from that of cloudy profiles (Sect 5.1).~~ is explored in more depth in Sect. 5.4.

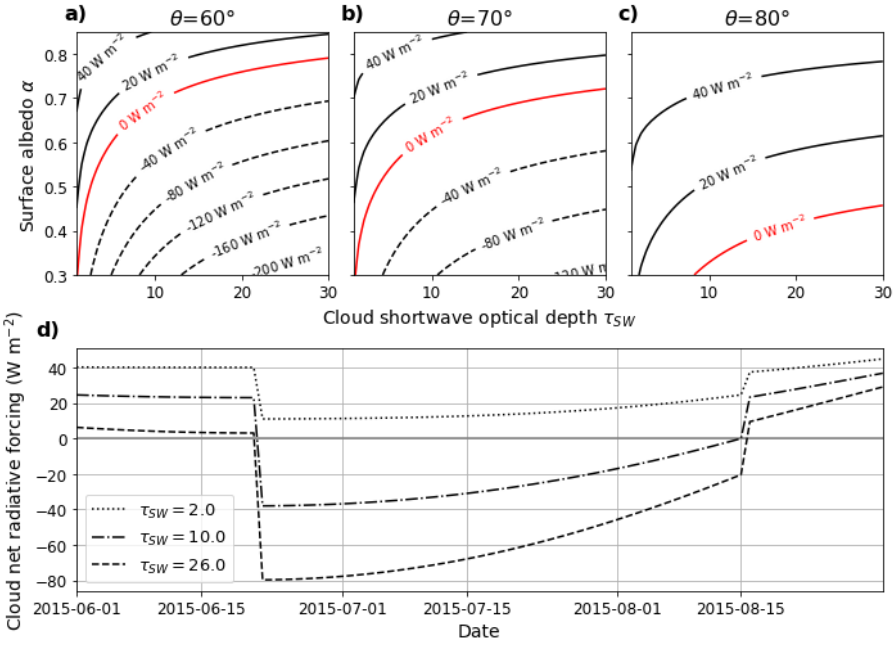

Figure 7. Panels a-c: iso-contours of net surface radiative forcing as a function of albedo and cloud shortwave optical depth for three different solar zenith angles (Eq. 8). Dashed black lines correspond to negative iso-contours, solid black lines to positive iso-contours, and red lines to the 0 W m^{-2} iso-contour. Panel d: Calculated evolution of the net surface cloud radiative forcing, for three different CODs (dotted line: $\tau_{SW} = 2$; dash-dotted line: $\tau_{SW} = 10$; dashed line: $\tau_{SW} = 26$), over the 2015 summer period. The summer variation of the albedo is constructed based on values from the NCAR Climate System Model (Weatherly et al., 1998), and the solar zenith angle values are daily averages at 82°N, 14°W (approximate position of the N-ICE ice camp).

5.4 ~~Contribution of the lowest cloud layer to the total column COD~~

5.4 Beyond N-ICE2015: estimating the summer cloud net radiative forcing at the surface

~~Optical depth5th percentile Median 95th percentile τ_{LW} 1.4 2 2.5 τ_{SW} 1.2 7.8 20.2 τ_{808} 0.5 0.9 1.9Statistical range (5th, 50th and 95th percentiles) of three different estimations of optical depth: τ_{LW} (from the downwards longwave flux), τ_{SW} (from the downwards shortwave flux) and τ_{808} (calculated from the IAOOS lidar profiles). For a robust comparison, τ_{LW} and τ_{SW} values considered here are interpolated on the IAOOS profile times. The percentiles are therefore established over 54 data points which correspond to the 54 IAOOS profiles.~~ The parametrisations introduced in Sect. 5.3 appear to work well when confronted with N-ICE radiative flux data: for CODs between 1.8 and 27.8, Eq. 7 reproduces the observed spread of downwards shortwave flux values at each zenith angle (Fig. 6). They can therefore be used to study the cloud net radiative forcing at the surface (netCF) and its dependence on solar zenith angle, albedo, and cloud optical depth. netCF is calculated according to the following equations:

~~Cloud optical depths measured by the IAOOS lidar correspond only to the lowest cloud layer, and not to the total column~~

$$\mathrm{CF}_{SW} = (1-\alpha)\cdot \mathrm{F}_0(\theta)\cdot(T_c(\theta,\tau_{SW},\alpha)-1)$$
$$\mathrm{CF}_{LW} \simeq 60\ \mathrm{W\ m^{-2}}$$
$$\mathrm{netCF} = \mathrm{CF}_{SW} + \mathrm{CF}_{LW} \quad (8)$$

with CF_{SW} the cloud shortwave radiative forcing and CF_{LW} the cloud longwave radiative forcing. These are counted as positive if they contribute to warm the surface, and negative if they contribute to cool it. In practice, CF_{LW} is positive and CF_{SW} is negative. Because CF_{LW} appears to depend little on surface temperature (Sect. ~~4.3). Here we attempt to evaluate the contribution of this lowest layer to the total column COD. This would allow better comparison of IAOOS CODs to existing satellite statistics. Furthermore, as seen~~ 5.3), it will be considered constant. T_c and F_0 are the cloud broadband shortwave transmission and the clear-sky downwards shortwave radiative flux respectively, which are calculated as in Sect. 5.3~~, total column shortwave COD is~~ .

The output of Eq. 8 is shown in Fig. 7a-c for varying values of the surface albedo α and the ~~quantity that most impacts the surface radiative balance. Equations 6 and 7 were inverted to calculate the broadband shortwave and longwave CODs~~ cloud shortwave optical depth τ_{SW} for zenith angle values $\theta = 60°$, $70°$ and $80°$. For each angle, the evolution is the same: netCF increases with α and decreases with τ_{SW}. Since CF_{LW} is considered to be constant, this is a shortwave effect. Optically thick clouds reflect more shortwave radiation than optically thin clouds, and the magnitude of this shortwave radiative cooling is larger over low-albedo surfaces. Indeed, since high-albedo sea ice reflects most of the incoming radiation, clouds have a lower absolute impact on the radiative balance over these surfaces. The solar zenith angle affects netCF in a similar fashion. For given values of α and ~~τ_{LW} from the~~ τ_{SW}, netCF increases with θ. The red line in Fig. 7a-c represents the $0\ \mathrm{W\ m^{-2}}$ iso-contour, and therefore delimits the regions of the (τ_{SW},α) plane in which clouds have a total net radiative cooling or warming effect. The higher the solar zenith angle, the smaller the region of net radiative cooling.

Equation 8 can also be used to estimate a summer cycle of netCF beyond the end of the N-ICE ~~opaquely cloudy SWd and LWd values at the time of the IAOOS profiles. In analysing the results, it must be taken into account that the longwave optical depth of any single cloud layer is smaller than its shortwave optical depth. The shortwave-to-longwave optical depth ratio depends on the microphysical properties of clouds (droplet phase,radius) and a precise determination would require the help of radiative transfer models. In this manner, Garnier et al. (2015) calculates $\tau_{532nm}/\tau_{12\mu m} \approx 1.8$ for ice particles with an effective diameter between 5 and 60 microns. We use this value as a rule of thumb to enable comparison between τ_{LW}~~ campaign period. In order to do that, values of θ and α must be chosen. While θ is easily calculated for a given date and location (here $82°$N, $14°$W, which is the approximate position of the N-ICE ice camp), ~~τ_{SW} and~~ α must be parametrised. We chose the four-level parametrisation for multiyear sea-ice used in the NCAR Climate System Model (Weatherly et al., 1998), which has been shown to agree well with SHEBA data (Perovich, 2002). In this model, cold snow is considered to have an albedo of 0.82, melting snow of 0.75, melting ice 0.5 and cold ice of 0.65. The transition between different surface types is naturally dependent on the specific location and year, but an approximate cycle can be constructed. Here the surface is set to be melting snow up to 21

June, melting ice from 21 June to 15 August, and cold ice from 15 August onwards. Indeed, the ~~IAOOS optical depths τ_{808}.~~ measured albedo was 0.74 (corresponding to melting snow) at the end of the N-ICE2015 campaign, i.e. on the 19 June 2015.

~~90% of τ_{LW} values obtained in this manner fall in the $1.4 - 2.5$ range (Table B1). It must be noted that these τ_{LW} values do not capture the optical depth of the whole column. Indeed, because cloud emissivity ϵ_c tends to 1 exponentially, high τ_{LW} values are likely to be underestimated. Instead, this τ_{LW} must be seen as the part of the cloud cover whose emitted radiation reaches the surface. Inverting Eq. (7) yields shortwave optical depths between 1.2 and 20.2, with a median of 7.8. This range shows much higher values than that of τ_{LW}, even when accounting for the longwave-to-shortwave ratio~~The results of this calculation are shown in Fig. 7d. Up to the 21 June 2015, only the optically thickest clouds ($\tau_{SW} = 26$) have a netCF which approaches zero, while optically thin clouds still contribute to warm the surface. This is ~~because the shortwave radiative flux is impacted by the whole cloud column, and not only the first few layers. IAOOS optical depths (τ_{808} in Table B1) are much lower than both τ_{LW} and τ_{SW}, with 90% of values between 0.5 and 1.9. In fact, the ratio $\tau_{808}/(1.8 \cdot \tau_{LW})$ has a median value of 0.22 (range $0.15 - 0.43$) , while τ_{808}/τ_{SW} has a median value of 0.11 (range $0.03 - 0.68$) . This means that first-layer clouds measured by IAOOS contribute around a quarter of~~ in accordance to the N-ICE2015 measurements (Sect. 5.3). As the surface transitions from melting snow to melting ice on the 21 June, the ~~optical depth of clouds which have a longwave radiative impact~~ netCF increases abruptly. This shows the important impact of α on the net cloud radiative forcing. However, τ_{SW} is almost as large a source of variability. The netCF for optically thin clouds ($\tau_{SW} = 2$) remains positive, i.e. they continue to warm the surface, while optically thick clouds ($\tau_{LW} = 26$) have a strong net surface cooling effect of -80 W m^{-2}. The netCF increases with the θ, and netCF values become positive for all τ_{SW} values with the surface transition to cold ice on the 15 August.

This approximate calculation of summer netCF exhibits negative values from the end of June to early August. This is coherent with the previous studies in the central Arctic Ocean, which showed that clouds exerted a cooling effect (i.e. negative radiative forcing) on the surface ~~, and 11% of the total cloud column.~~

~~While this value is low, it is~~ from the end of June to July (Shupe et al., 2006). It is also coherent with the observation that ~~SHEBA-measured total cloud thicknesses are up to 7 times higher than the IAOOS-measured first layer thickness (Sect. 4.2). Regardless of potential underestimations in IAOOS measurements, it strongly suggests that further cloud layers must be present at higher altitudes. Some of these, possibly cirrus clouds , would then have a shortwave but no longwave impact~~ during IAOOS, surface temperatures were lower in the absence of clouds for spring and autumn months, but not during the summer. However, netCF in these months also appears to depend strongly both on the surface and cloud type. Optically thin clouds may continue to warm the surface throughout the summer while thick, liquid water clouds will have a strong surface cooling effect. In considering the effect of clouds on the surface ~~. Furthermore, visual inspection of the relative humidity (RH) and temperature profiles obtained through radiosonde measurements during N-ICE supports the idea that the IAOOS lidar correctly identifies the first cloud layer and probably misses higher cloud layers~~radiative balance during the summer, it is therefore important to have an accurate estimation of COD and surface albedo. This strong variability in summer netCF may also contribute to explain that the 2 m temperature of cloudless profiles during IAOOS was not different at statistically significant level from that of cloudy profiles in June, July and August (Sect 5.1). Indeed, ~~strong temperature inversion and diminution of RH are most often present at the lidar-identified cloud top. Further inversions and high RH values are often present, marking higher~~

altitude cloud layers that are invisible to the lidarif summer netCF over the central Arctic Ocean were uniformly negative, for all clouds, the surface should be observed to be colder in the presence than in the absence of clouds.

6 Conclusions

The IAOOS field campaign (2014 - 2019) consisted in the deployment of instrumented buoys in the Arctic sea ice. In this study, the whole IAOOS lidar dataset was treated and analysed. This included correcting for window frost as outlined in Mariage (2015) and deconvoluting the signal to reduce the effects of receiver saturation in bright conditions. An algorithm was implemented to detect cloud layers and calculate their optical depth, either directly when applicable or through the IAB by assuming a constant lidar ratio. Surface radiative flux data from the N-ICE campaign, during which four IAOOS buoys were deployed, and from ERA5 reanalyses, was also exploited.

The results show a significant seasonal variation low number of profiles in some months causes some uncertainty on specific monthly cloud properties. However, the results show statistically significant differences in cloud cover and optical and geometrical properties of clouds over the seasonal cyclebetween the summer and April, November and December. Low cloud cover (i.e., with a base beneath 2 km) is found to be 76% globally over the course averaged over all months of the campaign. Monthly cloud frequency is minimum in March/April and November/December and over 85% from May - October, with two small maxima in June and October. First-layer clouds are geometrically thickest in October, and thinnest in the summer. This is likely linked to moisture intrusions from the Atlantic in early autumn. Lastly, first-layer cloud bases are found to be extremely low in all seasons: under 120 m in a vast majority of cases.

The IAOOS lidar detects multiple cloud layers at much lower rates than other instruments, because the first cloud layer usually dampens the signal completely. Total cloud optical and geometrical thicknesses from previous campaigns and satellite data are much larger than those measured by IAOOS, especially in the summer when multilayered clouds are known to be most common. We estimate from N-ICE radiometer measurements that the first layer COD measured by IAOOS accounted for 13% of the total column shortwave COD during the April-June 2015 period. The single-layer COD as measured by IAOOS is highest in October.

The surface impact of Arctic clouds is also seasonally variable. In October /November and Marchand November, clouds warm the surface: 2 m temperatures associated with cloudless profiles are up to 8 K colder than those associated with profiles containing at least one low cloud. However, there is no statistically significant difference in surface temperatures between cloudless and cloudy profiles in the summer.

Data from the IAOOS lidar deployed during the N-ICE campaign allowed us to identify two modes in the N-ICE measured netLW distribution in late spring/summer. The "radiatively clear" netLW mode, centered around -72 W m^{-2}, is associated with cloudless IAOOS lidar profiles, while the "opaquely cloudy" mode is centered around -11 W m^{-2} and is linked to cloudy lidar profiles. These are analogous to the well-known winter radiative modes, except that the opaquely cloudy mode is much more prevalent (over 80%) and that the two modes have a 60 W m^{-2} difference, compared to 40 W m^{-2} in the winter. Clouds exert a larger longwave warming in the summer than in the winter, probably linked to the higher proportion of liquid

water in clouds. Clouds in the spring/summer also have a shortwave cooling effect. This is shown to depend not only on solar zenith angle and albedo, but also strongly on COD.

~~The optically thickest clouds have a net radiative cooling effect around $\theta = 60$~~ During the N-ICE2015 April to June period clouds were observed exert a positive radiative forcing on the surface, with the cloud shortwave albedo effect cancelling out its longwave warming effect only for very large optical depths at zenith angles $> 60°$~~over unbroken sea ice, while most thinner clouds contribute to warm the~~. Over the full central Arctic Ocean summer cycle, it is estimated that optically thick clouds cause a negative radiative forcing of -80 W m^{-2} but that optically thin clouds continue to have a warming effect. It is therefore important to have a good estimation of whole-column COD in order to calculate the radiative effect of clouds on the surface. The compensation of the cloud longwave warming effect by the shortwave cooling effect explains that there is no clear difference in near-surface temperature between IAOOS cloudless and cloudy profiles during the summer months.

The measured surface radiative fluxes were compared to the output of the ERA5 reanalyses. ERA5 does not accurately reproduce the observed bimodality of the spring/summer netLW distribution. Indeed, it does not correctly identify cloudless periods during April and May (but not June). This issue should be investigated.

Over the period 2014-2019, the IAOOS buoys have delivered ~~1805~~ 1777 lidar profiles. Despite technical difficulties with both the lidar and the data analysis, this campaign has offered a medium-term 3-season picture of the Arctic lower troposphere above 82°N from ground-based measurement, which is an important complement to satellite data. These results help to broaden our understanding of the Arctic low cloud cover and its impacts on the surface. However, more measurements would be needed to further characterise Arctic clouds. In particular, combined ~~radiometer-lidar~~ radiometer-radar-lidar measurements would be crucial to allow the study of radiative impacts to be generalised to late summer and especially autumn, when clouds are optically thick and frequent.

Data availability. N–ICE2015 observational data sets are available from the Norwegian Polar Data Centre (https://data.npolar.no/dataset/) and are cited in the text (Hudson et al., 2016). IAOOS atmospheric data used in this paper are available upon request to the corresponding author and are available through the AERIS Data Portal at https://www.aeris-data.fr/. The ERA5 re–analysis products can be retrieved at http://apps.ecmwf.int/.

Appendix A: Determination of a 90% confidence interval for cloud occurrence frequency

Let us suppose that the event "presence of a cloud with base < 2 km in a given IAOOS lidar profile" follows a Bernoulli distribution of parameter p, with p the cloud frequency. This seems plausible given that the profiles are at least 6 hours apart, and the events can therefore be considered to be independent. We aim to determine a confidence interval for p based on:

1. Previous studies of clouds in the Arctic, which have shown that p is generally around 0.7;
2. The IAOOS measurements: for each month m, there are n_m profiles of which k_m contain at least one cloud with base < 2 km.

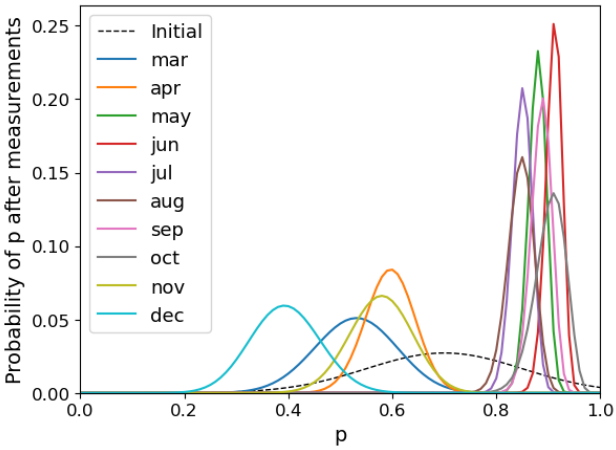

Figure A1. $\Pr(p|\text{meas})$ as a function of the cloud occurrence frequency p. The dashed black line corresponds to the a priori distribution. The updated distributions for each month (Eq. A1) are shown in colour.

From 1), an "a priori" probability distribution for p can be conceived: for example $\mathcal{N}(0.7, 0.15)$, normalised over the $[0,1]$ interval. Using the Bayes formula, the IAOOS measurements can then be taken into account to calculate an updated $\Pr(p|\text{meas})$ for each month m:

$$\Pr(p|\text{meas}) = \frac{\Pr(\text{meas}|p) \cdot \Pr(p)}{\Pr(\text{meas})} \tag{A1}$$

with

$$\begin{aligned} \Pr(\text{meas}|p) &= \mathcal{B}(k_m; n_m, p) \\ \Pr(\text{meas}) &= \sum_{p_i} \Pr(\text{meas}|p_i) \cdot \Pr(p_i) \\ &= \sum_{p_i} \mathcal{B}(k_m; n_m, p_i) \cdot \Pr(p_i) \end{aligned} \tag{A2}$$

where p_i are the possible values of the parameter p, and $\mathcal{B}(k; n, p) = \binom{n}{k} p^k (1-p)^{n-k}$ is the binomial probability mass function with parameters n and p. The results of this calculation are shown in Fig. A1, which synthesises the results of Sect. 4.1: the probability distributions for the months of May - October show significant overlap. However, they do not overlap at all with the November, December, March and April distributions, although these are much wider because of the lower number of measurements.

The 5th and 95th percentiles of the distribution of p determined through Eq. A1 can then be calculated to yield a 90% confidence interval.

Optical depth	5th percentile	Median	95th percentile
τ_{LW}	1.4	2	2.5
τ_{SW}	1.2	7.8	20.2
τ_{808}	0.5	0.9	1.9

Table B1. Statistical range (5th, 50th and 95th percentiles) of three different estimations of optical depth: τ_{LW} (from the downwards longwave flux), τ_{SW} (from the downwards shortwave flux) and τ_{808} (calculated from the IAOOS lidar profiles). For a robust comparison, τ_{LW} and τ_{SW} values considered here are interpolated on the IAOOS profile times. The percentiles are therefore established over 54 data points which correspond to the 54 IAOOS profiles. Individual errors carried over from measurement errors on LWd, SWd and T_{2m} are in the range $8-19\%$ (mean 11%) for τ_{SW}, and $8-23\%$ (mean 13%) for τ_{LW}.

Appendix B: Contribution of the lowest cloud layer to the total column COD

Cloud optical depths measured by the IAOOS lidar correspond only to the lowest cloud layer, and not to the total column (Sect. 4.3). Here we attempt to evaluate the contribution of this lowest layer to the total column COD. This would allow better comparison of IAOOS CODs to existing satellite statistics. Furthermore, as seen in Sect. 5.3, total column shortwave COD is the quantity that most impacts the surface radiative balance. Equations 6 and 7 were inverted using a numerical equation solver to calculate the broadband shortwave and longwave CODs τ_{SW} and τ_{LW} from the N-ICE SWd, LWd and temperature values at the time of the IAOOS profiles. Albedo was taken as fixed and equal to 0.8 in this calculation. The measurement errors of SWd, LWd and temperature (Sect. 2.2.1) as well as the choice of a fixed albedo create an error on τ_{SW} and τ_{LW} which is estimated through a Monte Carlo method. This error is no more than 19% for τ_{SW} and 23% for τ_{LW} (Table B1).

In analysing the results, it must be taken into account that the longwave optical depth of any single cloud layer is smaller than its shortwave optical depth. The shortwave-to-longwave optical depth ratio depends on the microphysical properties of clouds (droplet phase, radius) and a precise determination would require the help of radiative transfer models. In this manner, Garnier et al. (2015) calculates $\tau_{532nm}/\tau_{12\mu m} \approx 1.8$ for ice particles with an effective diameter between 5 and 60 microns. We use this value as a rule of thumb to enable comparison between τ_{LW}, τ_{SW} and the IAOOS optical depths τ_{808}.

90% of τ_{LW} values obtained in this manner fall in the $1.4-2.5$ range (Table B1). It must be noted that these τ_{LW} values do not capture the optical depth of the whole column. Indeed, because cloud emissivity ϵ_c tends to 1 exponentially, high τ_{LW} values are likely to be underestimated. Instead, this τ_{LW} must be seen as the part of the cloud cover whose emitted radiation reaches the surface. Inverting Eq. (7) yields shortwave optical depths between 1.2 and 20.2, with a median of 7.8. This range shows much higher values than that of τ_{LW}, even when accounting for the longwave-to-shortwave ratio. This is because the shortwave radiative flux is impacted by the whole cloud column, and not only the first few layers. IAOOS optical depths (τ_{808} in Table B1) are much lower than both τ_{LW} and τ_{SW}, with 90% of values between 0.5 and 1.9. In fact, the ratio $\tau_{808}/(1.8 \cdot \tau_{LW})$ has a median value of 0.22 (range $0.15-0.43$), while τ_{808}/τ_{SW} has a median value of 0.11 (range $0.03-0.68$). This means

that first-layer clouds measured by IAOOS contribute around a quarter of the optical depth of clouds which have a longwave radiative impact on the surface, and 11% of the total cloud column.

While this value is low, it is coherent with the observation that SHEBA-measured total cloud thicknesses are up to 7 times higher than the IAOOS-measured first layer thickness (Sect. 4.2). Regardless of potential underestimations in IAOOS measurements, it strongly suggests that further cloud layers must be present at higher altitudes. Some of these, possibly cirrus clouds, would then have a shortwave but no longwave impact on the surface. Furthermore, visual inspection of the relative humidity (RH) and temperature profiles obtained through radiosonde measurements during N-ICE supports the idea that the IAOOS lidar correctly identifies the first cloud layer and probably misses higher cloud layers. Indeed, strong temperature inversion and diminution of RH are most often present at the lidar-identified cloud top. Further inversions and high RH values are often present, marking higher altitude cloud layers that are invisible to the lidar.

Author contributions. JM performed the data treatment and analysis and prepared the manuscript. FR and JCR provided supervision, guidance and editing. JP led the IAOOS project and designed the lidar. VM constructed the lidar and treated its data.

Competing interests. The authors declare that they have no conflict of interest.

Acknowledgements. The authors acknowledge support from Stephen Hudson and Lana Cohen at the Norwegian Polar Institute and Von P. Walden at Washington State University for use of the N-ICE2015 dataset. They acknowledge their use of SHEBA data provided by NCAR/EOL under the sponsorship of the National Science Foundation. ~~They also acknowledge the support of EquipEx for the development of the IAOOS buoys.~~ This work was supported by the Equipex IAOOS (Ice Atmosphere Ocean Observing System) (ANR-10-EQPX-32-01), and by funding from the ICE-ARC program from the European Union 7th Framework Programme grant number 603887. Computer analyses benefited from access to IDRIS HPC resources (GENCI allocation A007017141) and the IPSL mesoscale computing center (CICLAD: Calcul Intensif pour le CLimat, l'Atmosphère et la Dynamique). This publication contains modified Copernicus Climate Change Service Information (2020). Neither the European Commission nor the ECMWF are responsible for any use that may be made of the Copernicus information or data in this publication.

References

ERA5 reanalysis data download, https://cds.climate.copernicus.eu/#!/search?text=ERA5&type=dataset.

http://www.iaoos-equipex.upmc.fr/fr/index.html.

SPCM-AQRH datasheet, 2018.

Blanchard, Y., Pelon, J., Eloranta, E. W., Moran, K. P., Delanoë, J., and Sèze, G.: A Synergistic Analysis of Cloud Cover and Vertical Distribution from A-Train and Ground-Based Sensors over the High Arctic Station Eureka from 2006 to 2010, Journal of Applied Meteorology and Climatology, 53, 2553–2570, https://doi.org/10.1175/JAMC-D-14-0021.1, 2014.

Bucholtz, A.: Rayleigh-scattering calculations for the terrestrial atmosphere, Optical Society of America, 34, 2765–2773, 1995.

Cesana, G., Kay, J. E., Chepfer, H., English, J. M., and de Boer, G.: Ubiquitous low-level liquid-containing Arctic clouds: new observations and climate model constraints from CALIPSO-GOCCP, Geophysical Research Letters, 39, L20 804, https://doi.org/10.1029/2012GL053385, 2012.

Chan, M. A. and Comiso, J. C.: Arctic Cloud Characteristics as Derived from MODIS, CALIPSO, and CloudSat, Journal of Climate, 26, 3285–3306, https://doi.org/10.1175/JCLI-D-12-00204.1, 2013.

Cohen, L., Hudson, S. R., Walden, V. P., Graham, R. M., and Granskog, M. A.: Meteorological conditions in a thinner Arctic sea ice regime from winter to summer during the Norwegian Young Sea Ice expedition (N-ICE2015), Journal of Geophysical Research: Atmospheres, 122, 7235–7259, https://doi.org/10.1002/2016jd026034, 2017.

Copernicus Climate Change Service (C3S): ERA5: Fifth generation of ECMWF atmospheric reanalyses of the global climate. Copernicus Climate Change Service Climate Data Store (CDS), https://cds.climate.copernicus.eu/cdsapp#!/home, 2017.

Curry, J. A., Ebert, E. E., and Herman, G. F.: Mean and turbulent structure of the summertime Arctic cloudy boundary layer, Quarterly Journal of the Royal Meteorological Society, 114, 715–746, 1988.

Curry, J. A., Rossow, W. B., Randall, D., and Schramm, J. L.: Overview of Arctic cloud and radiation characteristics, Journal of Climate, pp. 1731–1763, 1996.

de Boer, G., Eloranta, E. W., and Shupe, M. D.: Arctic Mixed-Phase Stratiform Cloud Properties from Multiple Years of Surface-Based Measurements at Two High-Latitude Locations, Journal of the Atmospheric Sciences, 66, 2874–2887, https://doi.org/10.1175/2009JAS3029.1, 2009.

Di Biagio, C., Pelon, J., Ancellet, G., Bazureau, A., and Mariage, V.: Sources, load, vertical distribution, and fate of wintertime aerosols north of Svalbard from combined V4 CALIOP data, ground-based IAOOS lidar observations and trajectory analysis, Journal of Geophysical Research: Atmospheres, 123, 2018.

Ding, Q., Schweiger, A., L'Heureux, M., Battisti, D. S., Po-Chedley, S., Johnson, N. C., Blanchard-Wrigglesworth, E., Harnos, K., Zhang, Q., Eastman, R., and Steig, E. J.: Influence of high-latitude atmospheric circulation changes on summertime Arctic sea ice, Nature Climate Change, 7, 289–295, https://doi.org/10.1038/nclimate3241, 2017.

Dong, X. and Mace, G. G.: Arctic Stratus Cloud Properties and Radiative Forcing Derived from Ground-Based Data Collected at Barrow, Alaska, Journal of Climate, 16, 445–461, https://doi.org/10.1175/1520-0442(2003)016<0445:ASCPAR>2.0.CO;2, 2003.

Fisher, R. A.: On the Interpretation of 2 from Contingency Tables, and the Calculation of P, Journal of the Royal Statistical Society, 85, 87, https://doi.org/10.2307/2340521, 1922.

Fitzpatrick, M. F., Brandt, R. E., and Warren, S. G.: Transmission of solar radiation by clouds over snow and ice surfaces: a parameterization in terms of optical depth, solar zenith angle, and surface albedo, Journal of Climate, 17, 266–275, 2003.

Garnier, A., Pelon, J., Vaughan, M. A., Winker, D. M., Trepte, C. R., and Dubuisson, P.: Lidar multiple scattering factors inferred from CALIPSO lidar and IIR retrievals of semi-transparent cirrus cloud optical depths over oceans, Atmospheric Mesaurement Techniques, 8, 2759–2774, 2015.

Graham, R. M., Rinke, A., Cohen, L., Hudson, S. R., Walden, V. P., Granskog, M. A., Dorn, W., Kayser, M., and Maturilli, M.: A comparison of the two Arctic atmospheric winter states observed during N-ICE2015 and SHEBA, Journal of Geophysical Research: Atmospheres, pp. 1–22, 2017.

Graham, R. M., Cohen, L., Ritzhaupt, N., Segger, B., Graversen, R. G., Rinke, A., Walden, V. P., Granskog, M. A., and Hudson, S. R.: Evaluation of six atmospheric reanalyses over Arctic sea ice from winter to early summer, Journal of Climate, 32, 4121–4143, https://doi.org/10.1175/JCLI-D-18-0643.1, 2019.

Hahn, C. J., Warren, S. G., and London, J.: The effect of moonlight on observation of cloud cover at night, and application to cloud climatology, Journal of Climate, 8, 1429–1446, 1995.

Hersbach, H., Bell, B., Berrisford, P., Hirahara, S., Horányi, A., Muñoz-Sabater, J., Nicolas, J., Peubey, C., Radu, R., Schepers, D., Simmons, A., Soci, C., Abdalla, S., Abellan, X., Balsamo, G., Bechtold, P., Biavati, G., Bidlot, J., Bonavita, M., Chiara, G., Dahlgren, P., Dee, D., Diamantakis, M., Dragani, R., Flemming, J., Forbes, R., Fuentes, M., Geer, A., Haimberger, L., Healy, S., Hogan, R. J., Hólm, E., Janisková, M., Keeley, S., Laloyaux, P., Lopez, P., Lupu, C., Radnoti, G., Rosnay, P., Rozum, I., Vamborg, F., Villaume, S., and Thépaut, J.-N.: The ERA5 global reanalysis, Quarterly Journal of the Royal Meteorological Society, 146, 1999–2049, https://doi.org/10.1002/qj.3803, 2020.

Hudson, S. R., Cohen, L., and Walden, V. P.: N-ICE2015 surface broadband radiation data, https://doi.org/10.21334/npolar.2016.a89cb766, 2016.

Intrieri, J. M., Fairall, C. W., Shupe, M. D., Persson, P. O. G., Andreas, E. L., Guest, P. S., and Moritz, R. E.: An annual cycle of Arctic surface cloud forcing at SHEBA, Journal of Geophysical Research, 107, 8039, 2002a.

Intrieri, J. M., Shupe, M. D., Uttal, T., and McCarty, B. J.: An annual cycle of Arctic cloud characteristics observed by radar and lidar at SHEBA, Journal of Geophysical Research, 107, 8030, 2002b.

Kambezidis, H. D., Psiloglou, B. E., Karagiannis, D., Dumka, U. C., and Kaskaoutis, D. G.: Meteorological Radiation Model (MRM v6.1): Improvements in diffuse radiation estimates and a new approach for implementation of cloud products, Renewable and Sustainable Energy Reviews, 74, 616–637, 2017.

Kay, J. E. and Gettelman, A.: Cloud influence on and response to seasonal Arctic ice loss, Journal of Geophysical Research, 114, D18 204, 2009.

Kay, J. E., L'Ecuyer, T., Chepfer, H., Loeb, N., Morrison, A., and Cesana, G.: Recent advances in arctic cloud and climate research, Current Climate Change Reports, 2, 159–169, 2016.

Koenig, Z., Provost, C., Villacieros-Robineau, N., Sennéchael, N., and Meyer, A.: Winter ocean-ice interactions under thin sea ice observed by IAOOS platforms during N-ICE2015: Salty surface mixed layer and active basal melt, Journal of Geophysical Research: Oceans, 121, 7898–7916, https://doi.org/10.1002/2016JC012195, https://agupubs.onlinelibrary.wiley.com/doi/abs/10.1002/2016JC012195, 2016.

Liu, Y., Key, J. R., Ackermann, S. A., Mace, G., and Zhang, Q.: Arctic cloud macrophysical characteristics from CloudSat and CALIPSO, Remote Sensing of Environment, 124, 159–173, 2012.

Lubin, D. and Vogelmann, A. M.: A climatologically significant aerosol longwave radiative effect, Nature, 439, 453–456, 2006.

Mann, H. B. and Whitney, D. R.: On a Test of Whether one of Two Random Variables is Stochastically Larger than the Other, Annals of Mathematical Statistics, 18, 50–60, https://doi.org/10.1214/aoms/1177730491, 1947.

Mariage, V.: Développement et mise en oeuvre de LiDAR embarqués sur bouées dérivantes pour l'étude des propriétés des aérosols et des nuages en Arctique et des forçages radiatifs induits, Tech. rep., Université Pierre et Marie Curie - Paris VI, 2015.

Mariage, V., Pelon, J., Blouzon, F., Victori, S., Geyskens, N., Amarouche, N., Drezen, C., Guillot, A., Calzas, M., Garracio, M., Wegmuller, N., Sennéchael, N., and Provost, C.: IAOOS microlidar-on-buoy development and first atmospheric observations obtained during 2014 and 2015 arctic drifts, Opt. Express, 25, A73–A84, https://doi.org/10.1364/OE.25.000A73, http://www.opticsexpress.org/abstract.cfm?URI=oe-25-4-A73, 2017.

Morrison, H., de Boer, G., Feingold, G., Harrington, J., Shupe, M. D., and Sulia, K.: Resilience of persistant Arctic mixed-phase clouds, Nature Geoscience, 5, 11–17, 2011.

Niemelä, S., Räisänen, P., and Savijärvi, H.: Comparison of surface radiative flux parametrizations, Part I: Longwave radiation, Atmospheric Research, 58, 1–18, 2001a.

Niemelä, S., Räisänen, P., and Savijärvi, H.: Comparison of surface radiative flux parameterizations: Part I: Longwave radiation, Atmospheric Research, 58, 1 – 18, https://doi.org/https://doi.org/10.1016/S0169-8095(01)00084-9, 2001b.

Nomokonova, T., Ebell, K., Löhnert, U., Maturilli, M., Ritter, C., and O'Connor, E.: Statistics on clouds and their relation to thermodynamic conditions at Ny-Alesund using ground-based sensor synergy, 19, 4105–4126, https://doi.org/10.5194/acp-19-4105-2019, 2019.

O'Connor, E. J., Illingworth, A. J., and Hogan, R. J.: A technique for autocalibration of cloud lidar, Journal of Atmospheric and Oceanic Technology, 21, 777–786, 2004.

Perovich, D. K.: Seasonal evolution of the albedo of multiyear Arctic sea ice, Journal of Geophysical Research, 107, https://doi.org/10.1029/2000jc000438, 2002.

Pithan, F. and Mauritsen, T.: Arctic amplification dominated by temperature feedbacks in contemporary climate models, Nature Geoscience, 7, 181–184, 2014.

Platt, C. M. R.: Lidar and radiometric observations of cirrus clouds, Journal of the Atmospheric Sciences, 30, 1192–1204, 1973.

Refaat, T. F., Ismail, S., Abedin, M. N., Spuler, S. M., Mayor, S. D., and Singh, U. N.: Lidar backscatter signal recovery from phototransistor systematic effect by deconvolution, Applied Optics, 47, 5281–5295, 2008.

Reno, M. J., Hansen, C. W., and Stein, J.: Global horizontal irradiance clear sky models: implementation and analysis, Tech. rep., Sandia National Laboratories, 2012.

Richardson, W. H.: Bayesian-Based Iterative Method of Image Restoration, Journal of the Optical Society of America, 62, 55–59, 1972.

Schmetz, P., Schmetz, J., and Raschke, E.: Evaluation of daytime downward longwave radiation at the surface from satellite and grid point data, Theoretical and Applied Climatology, 37, 136–149, 1986.

Shupe, M., Intrieri, J., and Uttal, T.: ETL Radar-Lidar 10-min Cloud Physical Properties. Version 1.0., https://doi.org/10.5065/D6MS3R4G, 2007.

Shupe, M. D. and Intrieri, J. M.: Cloud radiative forcing of the Arctic surface: the influence of cloud properties, surface albedo, and solar zenith angle, Journal of Climate, 17, 616–628, 2003.

Shupe, M. D., Matrosov, S. Y., and Uttal, T.: Arctic mixed-phase cloud properties derived from surface-based sensors at SHEBA, Journal of the Atmospheric Sciences, 63, 697–709, 2006.

Shupe, M. D., Walden, V. P., Eloranta, E., Uttal, T., Campbell, J. R., Starkweather, S. M., and Shiobara, M.: Clouds at Arctic Atmospheric Observatories. Part I: Occurrence and Macrophysical Properties, Journal of Applied Meteorology and Climatology, 50, 626–644, https://doi.org/10.1175/2010jamc2467.1, 2011.

Sotiropoulou, G., Tjernström, M., Sedlar, J., Achtert, P., Brooks, B. J., Brooks, I. M., Persson, P. O. G., Prytherch, J., Salisbury, D. J., Shupe, M. D., et al.: Atmospheric conditions during the Arctic Clouds in Summer Experiment (ACSE): Contrasting open water and sea ice surfaces during melt and freeze-up seasons, Journal of Climate, 29, 8721–8744, https://doi.org/10.1175/JCLI-D-16-0211.1, 2016.

Stramler, K., Genio, A. D. D., and Rossow, W. B.: Synoptically driven Arctic winter states, Journal of Climate, 24, 1747–1762, 2011.

Tjernstrom, M., Birch, C. E., Brooks, I. M., Shupe, M. D., Persson, P. O. G., Sedlar, J., Mauritsen, T., Leck, C., Paatero, J., Szczodrak, M., et al.: Meteorological conditions in the central Arctic summer during the Arctic Summer Cloud Ocean Study (ASCOS), Atmospheric Chemistry and Physics, 12, 6863–6889, https://doi.org/10.5194/acp-12-6863-2012, 2012.

Tjernström, M., Sedlar, J., and Shupe, M. D.: How Well Do Regional Climate Models Reproduce Radiation and Clouds in the Arctic? An Evaluation of ARCMIP Simulations, Journal of Applied Meteorology and Climatology, 47, 2405–2422, https://doi.org/10.1175/2008JAMC1845.1, 2008.

Tjernström, M., Leck, C., Birch, C. E., Bottenheim, J. W., Brooks, B. J., Brooks, I. M., Bäcklin, L., Chang, R., de Leeuw, G., Di Liberto, L., et al.: The Arctic Summer Cloud Ocean Study (ASCOS): overview and experimental design, https://doi.org/10.5194/acp-14-2823-2014, 2014.

Turner, D. D.: Arctic mixed-phase cloud properties from AERI Lidar observations: algorithm and results from SHEBA, Journal of Applied Meteorology, 44, 427–444, 2005.

Uttal, T., Starkweather, S., Drummond, J. R., Vihma, T., Makshtas, A. P., Darby, L. S., Burkhart, J. F., Cox, C. J., Schmeisser, L. N., Haiden, T., Maturilli, M., Shupe, M. D., De Boer, G., Saha, A., Grachev, A. A., Crepinsek, S. M., Bruhwiler, L., Goodison, B., McArthur, B., Walden, V. P., Dlugokencky, E. J., Persson, P. O. G., Lesins, G., Laurila, T., Ogren, J. A., Stone, R., Long, C. N., Sharma, S., Massling, A., Turner, D. D., Stanitski, D. M., Asmi, E., Aurela, M., Skov, H., Eleftheriadis, K., Virkkula, A., Platt, A., Førland, E. J., Iijima, Y., Nielsen, I. E., Bergin, M. H., Candlish, L., Zimov, N. S., Zimov, S. A., O'Neill, N. T., Fogal, P. F., Kivi, R., Konopleva-Akish, E. A., Verlinde, J., Kustov, V. Y., Vasel, B., Ivakhov, V. M., Viisanen, Y., and Intrieri, J. M.: International Arctic Systems for Observing the Atmosphere: An International Polar Year Legacy Consortium, Bulletin of the American Meteorological Society, 97, 1033–1056, https://doi.org/10.1175/BAMS-D-14-00145.1, 2016.

Walden, V. P., Hudson, S. R., and Cohen, L.: Norwegian Young Sea Ice Experiment (N-ICE) Field Campaign Report, https://doi.org/10.2172/1248935.

Walden, V. P., Hudson, S. R., Cohen, L., Murphy, S. Y., and Granskog, M. A.: Atmospheric components of the surface energy budget over young sea ice: Results from the N-ICE2015 campaign, Journal of Geophysical Research: Atmospheres, 122, 8427–8446, https://doi.org/10.1002/2016jd026091, 2017.

Wang, X. and Key, J. R.: Arctic surface, cloud and radiation properties based on the AVHHR Polar Pathfinder dataset. Part I: spatial and temporal characteristics, Journal of Climate, 18, 2558–2574, 2004.

Weatherly, J. W., Briegleb, B. P., Large, W. G., and Maslanik, J. A.: Sea Ice and Polar Climate in the NCAR CSM$*, Journal of Climate, 11, 1472--1486, https://doi.org/10.1175/1520-0442(1998)011 < 1472 : siapci > 2.0.co;2, 1998.$

Wendisch, M., Macke, A., Ehrlich, A., Lüpkes, C., Mech, M., Chechin, D., Dethloff, K., Velasco, C. B., Bozem, H., Brückner, M., Clemen, H.-C., Crewell, S., Donth, T., Dupuy, R., Ebell, K., Egerer, U., Engelmann, R., Engler, C., Eppers, O., Gehrmann, M., Gong, X., Gottschalk, M., Gourbeyre, C., Griesche, H., Hartmann, J., Hartmann, M., Heinold, B., Herber, A., Herrmann, H., Heygster, G., Hoor, P., Jafariserajehlou, S., Jäkel, E., Järvinen, E., Jourdan, O., Kästner, U., Kecorius, S., Knudsen, E. M., Köllner, F., Kretzschmar, J., Lelli, L., Leroy, D., Maturilli, M., Mei, L., Mertes, S., Mioche, G., Neuber, R., Nicolaus, M., Nomokonova, T., Notholt, J., Palm, M., van Pinxteren, M., Quaas, J., Richter, P., Ruiz-Donoso, E., Schäfer, M., Schmieder, K., Schnaiter, M., Schneider, J., Schwarzenböck, A., Seifert, P., Shupe,

M. D., Siebert, H., Spreen, G., Stapf, J., Stratmann, F., Vogl, T., Welti, A., Wex, H., Wiedensohler, A., Zanatta, M., and Zeppenfeld, S.: The Arctic Cloud Puzzle: Using ACLOUD/PASCAL Multiplatform Observations to Unravel the Role of Clouds and Aerosol Particles in Arctic Amplification, Bulletin of the American Meteorological Society, 100, 841–871, https://doi.org/10.1175/bams-d-18-0072.1, 2019.

Winker, D. M. and Vaughan, M. A.: Vertical distribution of clouds over Hampton, Virginia observed by lidar under the ECLIPS and FIRE ETO programs, Atmospheric Research, 34, 117–133, 1994.

Winker, D. M., Vaughan, M. A., and al: Overview of the CALIPSO mission and CALIOP data processing algorithms, Journal of Atmospheric and Oceanic Technology, 26, 2310–2323, 2009.

Winton, M.: Amplified Arctic climate change: What does surface albedo feedback have to do with it?, Geophysical Research Letters, 33, L03 701, 2006.

Woods, C., Caballero, R., and Svensson, G.: Large-scale circulation associated with moisture intrusions into the Arctic during the winter, Geophysical Research Letters, 40, 4717–4721, https://doi.org/10.1002/grl.50912, 2013.

Zygmuntowska, M., Mauritsen, T., Quaas, J., and Kaleschke, L.: Arctic clouds and surface radiation - a critical comparison of satellite retrievals and the ERA-Interim reanalysis, Atmospheric Chemistry and Physics, 12, 6667–6677, https://doi.org/10.5194/acp-12-6667-2012, 2012.